AD-A154 366 DEVELOPMENT AND APPLICATION OF A HIGH POWER ND-GLASS LASER INSTRUMENT(U) PENNSYLVANIA STATE UNIV UNIVERSITY PARK C L MERKLE ET AL. JAN 85 AFOSR-TR-85-0386 1/1

UNCLASSIFIED AFOSR-84-0048 F/G 20/5 NL

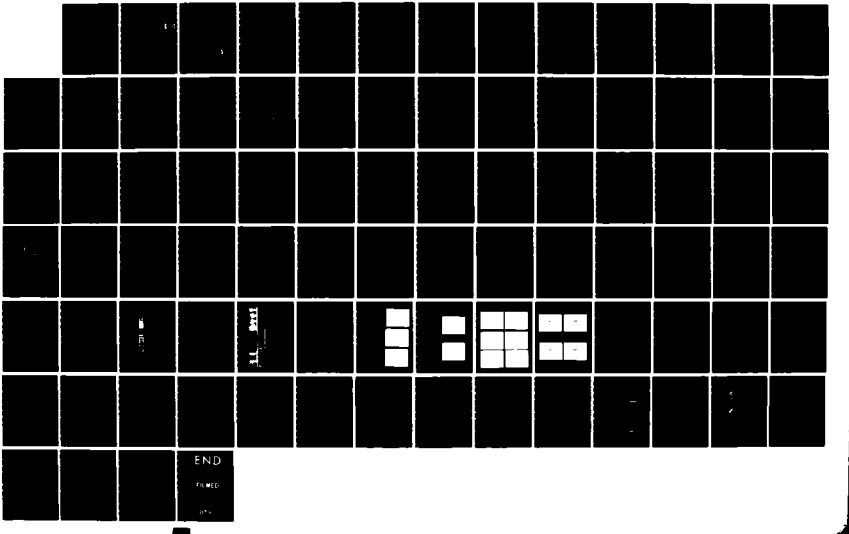

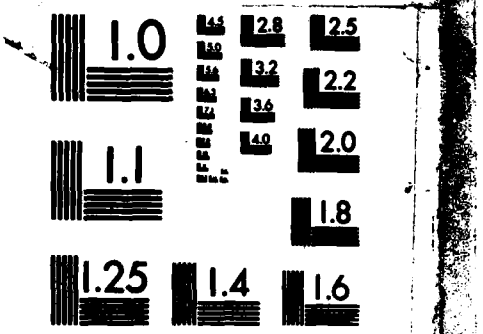

UNCLASSIFIED

SECURITY CLASSIFICATION OF THIS PAGE

REPORT DOCUMENTATION PAGE

AD-A154 366

1b. RESTRICTIVE MARKINGS

3. DISTRIBUTION/AVAILABILITY OF REPORT
Approved for Public Release;
Distribution is Unlimited.

2b. DECLASSIFICATION/DOWNGRADING SCHEDULE

4. PERFORMING ORGANIZATION REPORT NUMBER(S)

5. MONITORING ORGANIZATION REPORT NUMBER(S)
AFOSR-TR- 85-0386

6a. NAME OF PERFORMING ORGANIZATION
The Pennsylvania State University

6b. OFFICE SYMBOL (If applicable)

7a. NAME OF MONITORING ORGANIZATION
Same as #8

6c. ADDRESS (City, State and ZIP Code)
Mechanical/Aerospace Engineering Dept.
University Park, PA 16802

7b. ADDRESS (City, State and ZIP Code)
Same as #8

DTIC ELECTE JUN 3 1985 A

8a. NAME OF FUNDING/SPONSORING ORGANIZATION
AIR FORCE OFFICE OF SCIENTIFIC RESEARCH

8b. OFFICE SYMBOL (If applicable)
NA

9. PROCUREMENT INSTRUMENT IDENTIFICATION NUMBER
AFOSR-84-0048

8c. ADDRESS (City, State and ZIP Code)
BOLLING AFB, DC 20332-6448

10. SOURCE OF FUNDING NOS.

PROGRAM ELEMENT NO.	PROJECT NO.	TASK NO.	WORK UNIT NO.
61102F	2308	A1	

11. TITLE (Include Security Classification) DEVELOPMENT AND APPLICATION OF HIGH POWER ND-GLASS LASER INSTRUMENT

12. PERSONAL AUTHOR(S)
Charles L. Merkle & Thomas M. York

13a. TYPE OF REPORT	13b. TIME COVERED	14. DATE OF REPORT (Yr., Mo., Day)	15. PAGE COUNT
ANNUAL	FROM 01DEC83 TO 30NOV84	1985, January	84

16. SUPPLEMENTARY NOTATION

17. COSATI CODES		
FIELD	GROUP	SUB. GR.

18. SUBJECT TERMS (Continue on reverse if necessary and identify by block number)
BEAMED ENERGY
ADVANCED PROPULSION
LASER-GASDYNAMIC INTERACTION
HIGH POWER ND-GLASS LASER INSTRUMENT

19. ABSTRACT (Continue on reverse if necessary and identify by block number)

Research on the interaction between an incident laser beam and a flowing gas is described. The results include a discussion of the development and evaluation of a high power short wavelength source for experimental investigation of these interactions, as well as a summary of work on theoretical analysis of the interaction. The source uses an Nd-Yag oscillator followed by two high-gain amplifier stages to provide requisite power levels. At present, testing has been done with only the oscillator and the first-stage amplifier in place. Energy delivery for the first half of an anticipated ten millisecond duty cycle is closely in line with predictions and overall system performance looks promising. The analytical results describe initial results of the first detailed investigation of the stability characteristics of the interaction, as well as the first ever two-dimensional flowfield solutions for this problem.

DTIC FILE COPY

20. DISTRIBUTION/AVAILABILITY OF ABSTRACT
UNCLASSIFIED/UNLIMITED ☒ SAME AS RPT. ☐ DTIC USERS ☐

21. ABSTRACT SECURITY CLASSIFICATION
UNCLASSIFIED

22a. NAME OF RESPONSIBLE INDIVIDUAL
LEONARD H. CAVENY

22b. TELEPHONE NUMBER (Include Area Code)
(202) 767-4937

22c. OFFICE SYMBOL
AFOSR/NA

DD FORM 1473, 83 APR EDITION OF 1 JAN 73 IS OBSOLETE.

UNCLASSIFIED
SECURITY CLASSIFICATION OF THIS PAGE

85 4 23 046

Annual Report

on

DEVELOPMENT AND APPLICATION OF A HIGH POWER ND-GLASS LASER INSTRUMENT

Submitted to:

Dr. L. H. Caveny
Air Force Office of Scientific Research
Directorate of Aerospace Sciences
Bolling Air Force Base, D.C. 20332

by

Dr. Thomas M. York
Aerospace Engineering Department
814-863-0602

Dr. Charles L. Merkle
Mechanical Engineering Department
814-863-1501

The Pennsylvania State University
University Park, PA 16802

January 1985

Annual Report

on

DEVELOPMENT AND APPLICATION OF A HIGH POWER ND:GLASS LASER INSTRUMENT

Submitted to:

Dr. L. H. Caveny
Air Force Office of Scientific Research
Directorate of Aerospace Sciences
Bolling Air Force Base, D.C. 20332

by

Dr. Thomas M. York
Aerospace Engineering Department
The Pennsylvania State University
University Park, PA 16802
814-863-0602

January 1985

b. Research Objectives

The original proposal for research on high power Nd:glass heating of gases listed three general tasks that were to be accomplished during the one-year study.

1. Demonstrate laser oscillator and first stage amplifier operation at 1.06 μm at power levels up to 1 KW.
2. Identify the geometric configuration and pressure levels for gas absorbtivity measurements at 1.06 μm.
3. Establish physical principles that approximate the interaction between a short duration, high power laser beam and a gas, in order to guide experiments. Obtain representative preductions from one-dimensional laser absorption analysis at 1.06 μm.

However, it had been identified early in the contract year that this research effort would not be continued beyond the one year funded period. Accordingly, there was de-emphasis of the tasks 2 and 3, with greater emphasis on task 1: determination of amplifier performance for a mode locked oscillator output.

c. Status of Research Effort

1. Experiment (Zich)

Studies were made of several aspects of the physics involved in the operation of a high power, mode-locked laser. The theory of mode-locking and the methods of achieving mode-locking in a system were investigated and the results were presented in a report (Appendix A). Mode-locking and simultaneous mode-locking and Q-switching are of interest because the peak powers obtained are higher than the powers available from CW operation. The higher peak powers yield greater efficiency in frequency doubling and in extracting energy from an amplifier. The spacing between the mode-locked pulses is of the order of 10ns, which allows some time for repopulation of the lasing level as well as offering the possibility of temporal resolution in diagnostics work or of statistical signal averaging. The diagnostics possibilities are dependent on a fast detection and recording system.

The effect of Nd doping levels in glass rods was examined with regard to producing a uniform beam. At higher doping levels, absorption of the pump light in the periphery of the rod results in less pumping of the rod center and lower intensity at the center of the beam. In extreme cases this yields an annular intensity distribution (Appendix A).

A study of thermal effects in laser rods was carried out. The report of this work is included as Appendix B. The study was undertaken anticipating heating effects would occur in the amplifier rod with relatively long pump time with 10 ms bursts. Thermal

lensing and thermal birefringence also occur in quasi-cw or multi-pulse systems. Thermal effects could be significant in the oscillator as well. Thermal effects cause distortion of the beam, which could lead to unacceptable divergence and/or uneven heating of a working fluid. In addition, frequency doubling or diagnostic applications require a uniform beam for acceptable performance.

The primary work accomplished under this contract was the design, assembly, and operation of an Nd:YAG/Nd:glass laser system capable of operating mode-locked or mode-locked/Q-switched for up to 10ms. This involved a survey of laser and component suppliers to determine possible vendors for the system components and for additional equipment such as detectors, power supplies, oscilloscopes, etc. needed to operate and characterize such a system. Components were selected to meet the system specifications. An equipment budget is presented in Appendix C. There were two major delays in the delivery of equipment to the laboratory. The first of these was in the construction of the power supply for the laser amplifier. The second delay was in the Tektronix 7104 oscilloscope. The design and anticipated performance of the laser system is detailed in Appendix D.

A Quantronix model 116R-O/ML-QS Nd:YAG laser was chosen for the oscillator. This laser offers the possibility of running CW, CW mode-locked, CW mode-locked/Q-switched, repetitively Q-switched, or single shot Q-switched. The oscillator is set up to run in the TEM_{oo} mode with an averaging power of 14W CW, and an average power 10W CW mode-locked. The beam divergence is 2.2mr. Each mode-locked pulse is 100 ps long and is 100nJ. The spacing between pulses is 10ns.

Full specifications of the oscillator are given in Appendix D. The output of the oscillator was observed to insure that mode-locking and Q-switching were occurring and that the frequency of both processes was as expected (Appendix E).

The amplifier was an Apollo Lasers model 26520 S amplifier system. The pump length of the amplifier head is 12" (~15" rod). The power supply has a total capacitance of 4800μf which gives an energy storage of 57,624J at a charging voltage of 4.9kV and 83,544J at 5.9kV (maximum). This is arranged in two banks of ten 240μf capacitors. The rod is pumped by two helical 6" Xenon flashlamps (Spaceglass), each flashlamp driven by one of the banks of ten capacitors. A network inductors lengthens the discharge time to enable the flashlamps to pump the amplifier rod for 10ms. The power supply is constructed so the pumping time may be changed in ~1 ms increments from 1ms to 10ms by adding or detaching capacitors from the lamps. Each capacitor is worth about 1ms of driving time.

The amplifier rods are Kigre Q-246 silicate glass, 15" x 3/8" diameter, with 6° beveled ends, 3% doped. Silicate glass was chosen because of the good wavelength match with Nd:YAG. The fluorescence peak of Neodymium in Yag occurs at 1.064μm. In silicate glass the peak is at 1.062μm, 0.002μm different from Nd:YAG, whereas in phosphate glass the is at 1.054μm, 0.010μm away from the peak of Nd:YAG. With the peak fluorescence wavelengths 0.010μm apart the gain available from phosphate glass is considerably less than it would be if the wavelengths were the same. Because phosphate glass in general offers higher gains than silicate glass, it has been proposed that the large wavelength difference can be offset by the

higher gain of phosphate glass when designing Nd:YAG/Nd:glass systems. Tests on a second laser system indicate that the wavelength difference is still significant, and the silicate glass is a more appropriate amplifier for Nd:YAG than phosphate glass. Silicate glass has an advantage because it is harder than phosphate glass and more likely to stand the stress of high power pumping without damage.

The oscillator/amplifier system was set up as diagrammed in Appendix D. The oscillator, 10X beam expander (Special Optics model 52-25-10X-1.06), and amplifier were arranged linearly (straight beam path, no mirrors) with about 1 meter between oscillator output mirror and beam expander, and about 2.5 meter between oscillator and amplifier. The spacing between the components is large to inhibit feed back and to reduce divergence of the system. Beam tubes enclosed the beam path between components and the beam path to the detection system. This was done to reduce the effects of dust on the system and to increase the safety of the people working with the laser.

The investigation of the system performance was carried out using energy meter and photodiode measurements. The overall gain measurements were done by measuring the amplifier input laser power with a Coherent model 201 power meter, then calculating the input energy using the amplified burst length as measured by photodiode trace and energy = power x time. A Quantronix model 500 energy receiver was used to measure the laser energy output of the amplifier. There was no means to input oscillator energy into the amplifier for just the time when the amplifier flashlamps were being driven, so the electromechanical shutter on the oscillator was rigged to allow ~1ms

(shortest time interval possible) of CW mode-locked emission into the amplifier. During this time the amplifier flashlamps were fired. The oscillator energy which went through the amplifier when the flashlamps were not fired was measured, and this background was subtracted from the energy measured when the amplifier lamps were fired. This was done because the amplifier lamps were driven for a maximum of 10ms, and the unamplified oscillator energy passing through the rod before and after the lamps were fired was significant. Measurements were started using 1 capacitor/flashlamp (~1ms setting) and additional capacitors were added as the study progressed.

The average CW mode-locked output of the oscillator at the point of input into the amplifier was 6.82W. This is reduced from 10.5W output of the oscillator because of off-optimum operation and losses. The 6.82W is the power of the entire beam. Tests with a 3/8" (rod diameter) aperture in front of a power meter at the rod location have shown that because of divergence only an average power of 3.51 W were input to the amplifier rod. The mode-locked and the Q-switched pulses were observed with a Ford Aerospace L4501 photodiode. The frequency stability and the amplitude stability of the pulses was excellent. The output power of the oscillator was observed to fluctuate slightly (5%) on the 10s scale. This is a result of arc lamp fluctuations.

There were problems with the amplifier system power supply. At amplifier run times above 5 capacitors/flashlamp (of a total of 10 capacitors/flashlamp possible), at 4.9kV, the magnetic forces on some components in the power supply caused these components to twist and

to break free of their mounts. This required a significant delay to design fabricate and install stronger replacement mounts.

Energy and gain measurements were made for different numbers of driving capacitors and different charging voltages. Using one driving capacitor/flashlamp at 4.9kV the average energy output was 0.220J the average gain under these conditions was 79.58. For two capacitors/flashlamp the output was 0.433J and the gain was 61.26. With three capacitors/flashlamp the energy was 0.684J and the gain 70.65. Five capacitors/flashlamp gave an average of 0.938J and a gain of 59.00. Using seven capacitors/flashlamp produced an energy yield of 1.05J and a gain of 41.97 (58.42 for a 5ms period). Ten capacitors/flashlamp gave an energy of 1.16J and a gain of 32.37 (63.99 for a 5ms period).

In an effort to obtain higher output energies and gains the amplifier system was modified to charge to a maximum of 5.9kV instead of 4.9kV. This was done after consultation with Apollo Lasers and Space Glass (the flashlamp manufacturer). Measurements taken at increasing voltages using one capacitor/flashlamp showed a dramatic increase in energy output and gain as voltage increased. At 4.9kV the energy was 0.220J and the gain was 79.50. Increasing the voltage to 5.5kV gave an energy of 0.345J and the gain increased to 94.26. At 5.9kV, the energy was 0.557J with a gain of 152.25. With a power input of 3.51W, this indicated 0.53KW amplifier output; alignment to reduce divergence should provide the desired 1KW power level.

Other observations made of the amplifier output burst revealed unique characteristics of the burst. Photodiode observation showed a model structure with a temporal separation of 200us - 250us

(Appendix E). These were not related to the mode-locked pulses. The mode-locked pulses were observable within the mode structure when the time scale was decreased. The pulsed structure in the burst appears under a number of different conditions, including attenuation of the beam using a beam splitter and a dispersing lens. A possible explanation is that the pulsing in the burst is related to relaxation oscillations in the rod; this was described by W. Kochner (Solid-State Laser Engineering) although relaxation oscillations are commonly at a 50kHz - 200kHz frequency rather than 4kHz - 5kHz. Another possibility investigated was fluctuations in flashlamp output due to current or voltage fluctuations. The voltage and current driving the flashlamps showed no oscillations which might be related to the pulsation. (Appendix E)

Photodiode records of the amplified burst while the system operated for 10ms showed that the amplifier would amplify for only about 5 ms, although the flashlamps, as indicated by current and voltage records, pumped the rod for a full 10ms. This tendency is evident for all run times greater than 5ms. At run times less than 5ms the amplifier amplifies for the entire time period. The cause of this phenomena is not yet understood. A 14" x 3/4" ED-2 silicate glass rod was borrowed from Apollo Lasers to test whether the pulsation and gain decay effects originate in the type of silicate glass used in the amplifier rod. The test was not entirely successful, apparently due to poor pumping of the rod resulting from absorption in the thicker rod. The ED-2 rod did amplify at a very low level (gain 20 - 25), and the amplified burst shows a smooth structure with no pulsations. At the same 3kV voltage, the Q-246 silicate glass rod did not demonstrate the fluctuating output evident at higher charging voltages.

As a data recording system for the laser system, a number of alternatives were considered. There is not yet a digitizer or oscilloscope with fast enough response to capture the 100ps pulses without distortion. A fast programmable digitizer would allow observation of the pulse shape based on the known electronic characteristics of that digitizer, but budget constraints did not permit this option. A fast oscilloscope was chosen after a demonstration of the oscilloscope showed the mode-locked pulses would not be distorted to uselessness by the device. A more complete report on detection systems is included in Appendix F.

Recommendations

The ~200us pulsations in the burst structure should be investigated further. The test using an ED-2 amplifier rod seemed promising, but a test with an ED-2 rod of the same size and end bevels as the present Q-246 rod would be more conclusive. Additional tests with identical Q-246 and ED-2 rods might also indicate the cause behind the gain decoy after 5ms. Comparison with results from a phosphate glass rod would establish gain factors for phosphate and silicate glasses amplifying Nd:YAG, as well as providing more data on the use of Nd:glass for long burst/pulse amplification. Studies of the gain and energy output of the present system should be pursued to determine the benefit of driving the amplifier flashlamps at higher voltages. Comparison should be made between the efficiency of fewer long bursts versus shorter bursts.

2. Theory (Breisacher)

The mechanism of a continuous-wave laser propulsion system and the potential uses of such a system were outlined. The formulation of a one-dimensional model for an absorber and nozzle combination, as developed by Merkle and Gulati was examined in detail. The problem of divergence of their solution for the absorption chamber being radiated at short wavelengths was considered. A plan of attack was developed utilizing the new numerical method of Keefer, Peters, and Crowder to obtain a complete numerical solution for an absorber and nozzle wavelengths of .53μm and 1.06μm at incident laser intensities on the order of 4.0×10^7 W/m^2.

The results of this effort are as follows. First, the representation of the thermodynamic properties of hydrogen under the influence of short wavelength radiation was completed. The second major effort involved utilizing Keefer's numerical integration techniques to the absorption problem for short wavelength. The results were partially successful. There was limited information in the literature on the details of Keefer's techniques. However, the present effort did succeed in achieving a satisfactory solution for a test case reported by Keefer. However, exact reproduction of his results was not obtained. The incident intensity was a factor of 3 different, while the position of real temperature occurred densities. This effort was terminated with the graduation (B.S. in Aerospace Engr.) of Mr. Breisacher in June 1984.

d. Written Publication in Technical Journals

None

e. Professional Personnel Associated with Research Efforts

T. M. York, Principal Investigator Professor of Aerospace Engineering	15%, 9 mths. 25%, 3 mths.
R. Zich, Research Assistant Mechanical Engineering	75%, 12 mths.
K. Breisacher, Undergraduate Assistant	0%, 9.0 mths.

f. Interactions

(Spoken papers)

1. A High Power Nd:glass Laser Instrument for Advanced Propulsion and Diagnostics AFOSR/AFRPL Rocket Propulsion Research Meeting, 12 - 15 March 1984, Lancaster, CA.

APPENDIX A

DETAILED INVESTIGATION OF LASER OPTICAL TECHNIQUES

A. Mode Locking

A further study of mode locking and mode-lockers has been made. Mode locking is a process which restricts the axial modes of a laser so they have a common phase relationship. The term "axial modes" is a reference to the ability of lasers to support a number (anywhere from three to several hundred) of closely spaced but discrete frequencies. The explanation of this is as follows: the toal gain of a lasing medium, $\tilde{g}(\omega)$, is a function of the single pass traveling-wave gain $\tilde{g}_1(\omega)$. There is a phase shift during amplification which comes from a term $n_o\omega L/c$ in $\tilde{g}_1(\omega)$ where n_o = index of refraction of the cavity, ω = center frequency of the laser line, L = cavity length, and c = speed of light ($2n_o\omega L/c$ for a round trip in the cavity). Because of this term the gain is high only for frequencies which fulfill the condition.

$$2n_o\omega L/c = 2\pi q \qquad q = 0, 1, 2, \ldots$$

Thus, the frequencies are[1]:

$$f = \omega/2\pi = qc/2n_oL$$

with the additional stipulation that the frequencies lie within the atomic linewidth of the laser transition. The frequency spacing between two adjacent axial modes is

$$f = f_{q+1} - f_q = c/2n_cL$$

In practice n_c is often taken to be equal to unity for purposes of

estimating the pulse lengths and the frequency spacing. In other words, since the frequency linewidth of the laser transition is finite, a range of frequencies can be supported by this transition. The allowed frequencies are then determined by the requirement that an integral number of half wavelengths of the given frequency must exist in the cavity, otherwise destructive interference will occur and the wave will be extinguished. These frequencies constitute the axial modes.

The peak intensities versus frequencies of the modes for a given transition determine a Gaussian envelope centered on the midpoint frequency of the transition. Individual mode intensities are given by[2]

$$I = I_c \exp \{-4 \ln [\, 2(n\omega_c/\Delta w)^2]\}$$

where I = mode intensity at line center

ω_c = mode separation

$\Delta\omega$ = half maximum bandwidth for mode amplitudes

n = mode number, 0 to $(N-1)/2$ (N = the number of modes supported)

Mode locking is a method by which the initial phases of the axial modes emitted by a laser are set to a common value, i.e. only photons which start circulating in the cavity at the same time are permitted to stimulate emission of further photons (be amplified) and be output. This results in the output of the laser being a series of short duration, high peak power pulses rather than being output continuously at a lower maximum power. For a cw-driven laser the mode-locked output is a continuous train of pulses. In the case of a pulsed laser each pulse is an envelope for a train of mode-locked pulses and the peak pulse

power is increased. This mode locking is done by inserting either an amplitude (AM) modulator or a phase (FM) modulator into the laser cavity. Considering a general expression for an electromagnetic field.

$$e(t) = \sum_{\frac{-(N-1)}{2}}^{\frac{(N-1)}{2}} E_n \exp \{i [(\omega + n\omega_c) t + \phi_n]\}$$

where ω = center frequency of the laser transition

ω_c = mode separation

n = mode number

ϕ_n = initial phase

Mode locking forces all the ϕ_n to a common value of $\phi_i \pm 2n\pi$. The output of the laser with respect to time and frequency is no longer similar to that shown in Figure 1, for a non-mode-locked laser, but is like that of Figure 2. [3]

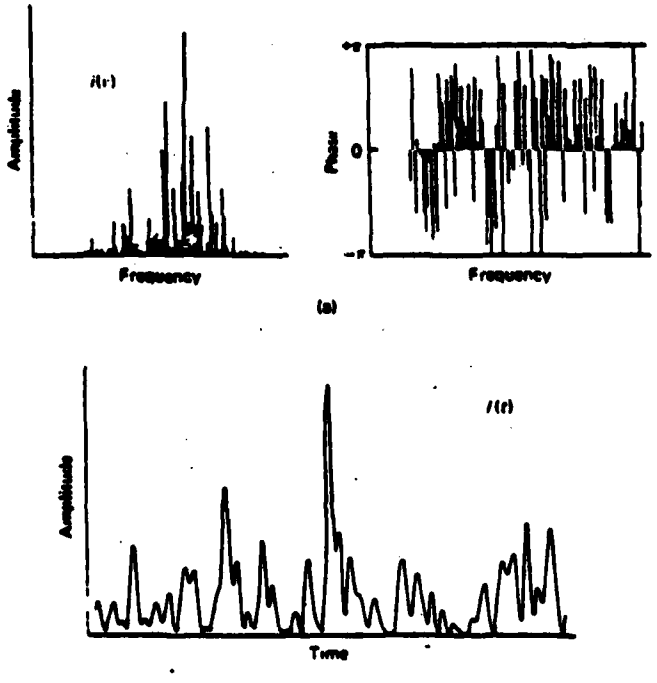

Fig. 1. Signal of a non-mode-locked laser.

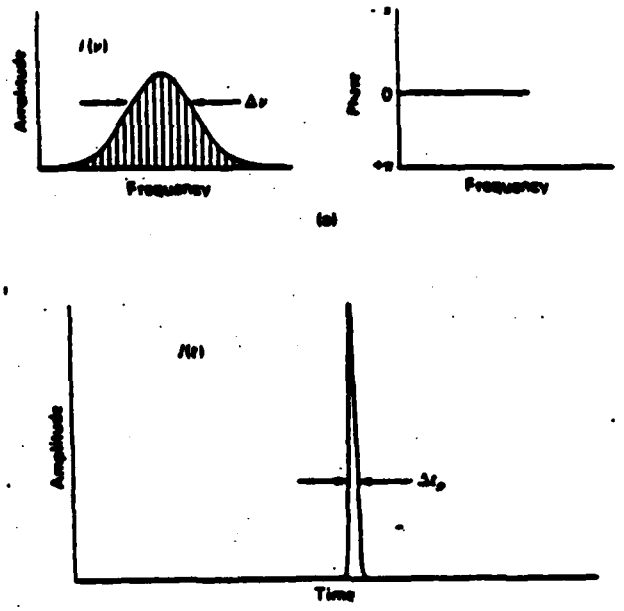

Fig. 2. Signal structure of an ideally mode-locked laser.

In the type of system under consideration, a cw-driven Nd:YAG oscillator has an acoustooptic or electrooptic device placed in the laser cavity to modulate the circulating light, preventing light modes without the chosen common initial phase from being amplified. This modulation is periodic with a frequency equal to the frequency separation of the axial modes ($f = c/2L$ using $n = 1$), or equal to one-half this frequency.

Amplitude modulation, sometimes known as loss modulation, works by introducing into the cavity a time-varying transmission. Since the light requires a time of $2L/c$ to make a round trip of the cavity, a transmission maximum which occurs every $2L/c$ will pass the light (modes) with a common initial phase or starting time, and block the rest of the light. Most of the population inversion then depletes to amplify the common-phase modes, yeilding a short, high peak power pulse. Materials

in common use today for AM mode-lockers have transmission maxima which occur twice during one period of the driving frequency and are driven at a frequency equal to one-half the axial mode separation to provide the correct frequency of transmission maxima. In practice mode-lockers are placed as close as possible to the 100% mirror to avoid the problem of having to time the modulation to pass the light pulse both coming and going. The pulse passes through the mode-locker, reflects from the mirror, and passes back through the mode-locker during one transmission maxima. The round trip transmission function for AM mode-locakers is given by[4]

$$T(t) = \exp\left(-\delta_{AM}^2 \omega^2 t^2\right)$$

where δ_{am} = AM modulation index

The second method of mode locking a laser is phase modulation. Phase modulation uses an electroopptic device in the laser cavity to cause a frequency shift in light which passes through the modulator except light which passes through when the frequency shifting property is zero. The modulator does this shifting by introducing a sinusoidally varying phase perturbation $\delta(t)$ into the cavity. The shift in frequency is proportional to $d\delta/dt$. This causes an ambiguity because the light pulse may pass through the modulator at either of the two extrema of $\delta(t)$. In operation only one of the extrema acts as the gate at a time, as larger losses in the cavity would occur otherwise. The driving frequency of a phase modulator is thus equal to the axial mode spacing rather than to half the axial mode spacing as is the case with amplitude modulation. Repeated passes

of light through the modulator (other than at $d\delta/dt = 0$) results in the frequency being shift further, eventually being pushed outside the bandwidth which can be amplified by the active medium. One author (Koechner[5]) states that this frequency shift is due to a Doppler shift, while others (Kuizenga[6]) hold that the shift is due to a linear frequency shift (chirp). The round trip transmission function is[7]

$$T(t) = \exp\left(\pm i\delta_{FM}\omega^2 t^2\right)$$

where δ_{FM} = peak phase retardation

Most commercial mode-lockers used on Nd:YAG lasers are of the acoustooptic variety because higher optical quality is available for this type of device at present, and Nd:YAG lasers are very sensitive to the optical quality of anything put in the laser cavity. Also, the acoustooptic mode-lockers are easier to modulate than electrooptic mode-lockers.[8]

B. Simultaneous Mode Locking and Q-Switching

In current mode-locked Nd:YAG laser systems the user may choose between a mode-locked system and a mode-locked and Q-switched system. During pumping, a population inversion occurs in the laser medium. When the population inversion reaches a certain threshold level, spontaneous emission will be able to deexcite enough ions to deplete the inversion and lase. Q-switching prevents any spontaneously emitted light from circulating in the cavity and depleting the inversion.

In this manner the inversion is allowed to build up to a much higher level, storing more energy. When lasing is allowed to occur the pulse will be of higher energy than that from a unswitched system, both because the population inversion is initially higher and because the greater number of ions deexciting gives a higher photon density which deexcites a greater percentage of the inversion. Also, because of the high gain the inversion is deexcited in a short period of time (although not short compared to mode-locked pulse lengths). Because of the high peak power of a Q-switched pulse compared to that of unswitched pulses the Q-switched pulse is refered to as a giant pulse. The evolution of a Q-switched pulse is shown in Figure 3.[9]

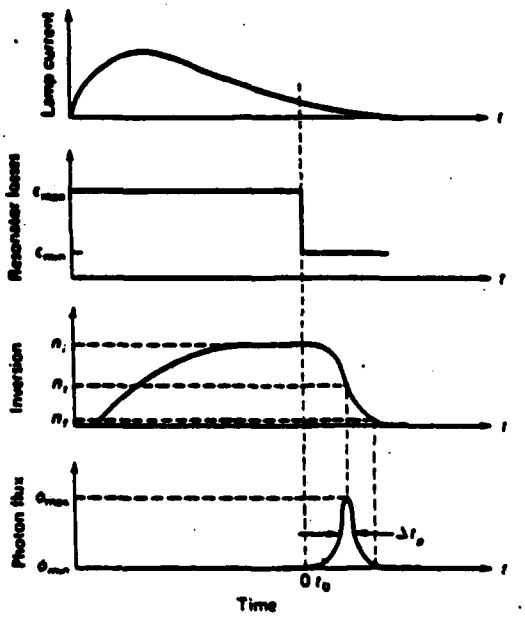

Fig. 3. Development of a Q-switched laser pulse. Shown is the flashlamp output, resonator loss, population inversion, and photon flux as a function of time.

The Q-switch prevents light circulation in the cavity by greatly increasing the energy loss per cycle. Since the quality (Q) factor is the ratio of energy stored in the cavity to the energy lost per cycle this lowers the Q of the cavity (also known as Q-spoiling)(10). The spoiling can be done either mechanically as with rotating mirrors or electrooptically as with Pockels cell polarizers.

Combining mode locking and Q-switching gives much greater peak power pulses than either process alone gives.[11] Simultaneous mode-locking and Q-switching results in a mode-locked train of pulses under a Q-switched envelope. Cohen [12] has reported pulses with a peak power of a megawatt with a repitation rate of up to 800 Hz. Kuizenga, et al.[13] experimented with simultaneous mode locking and Q-switching. They reported obtaining pulse lengths as low as 100 ps, however, they also found that the steady state mode-locked pulse length could only be obtained if the population inversion before Q-switching is close to threshold. This gives low peak power pulses and problems with pulse to pulse stability.

The repitation rate would be a definite problem in trying to incorporate both Q-switching and mode locking into the proposed laser system. Current repetition rates for Q-switches are around 1kHz for a gain in peak pulse power.[14] Since the desired pulse repetition rate for the oscillator is 100 MHz, attempting to Q-switch the system would result in a degradation of performance.

C. Effects and Effectiveness of Laser Rod Doping

One of the qualities desired in a solid state laser is efficient use of the oscillator and amplifier rods from a pumping standpoint. Since light from the pumping lamp(s) is absorbed by both the neodymium and the YAG or glass host, the closer one gets to the axis of the rod, the less energy is available to excite the neodymium. This leads to a radial profile in which the emission is most intense near the outer edge of the beam. In severe cases an annular emission occurs, with little or no lasing from the center of the rod. The Naval Research Laboratory did studies using 1/4" diameter Nd-doped glass rods. For a rod with 9% doping an intensity variation of 36:1 from edge to center of the rod was found. For a rod with 3% doping a variation of 6:1 from edge to center was observed.[15] While a beam with a uniform radial intensity profile is not necessary for propulsion applications, design criteria used in obtaining such a beam can be used in systems which do require a fairly uniform beam (eg. Thompson scattering plasma diagnostics) and in getting the most efficient rod use for the system under study.

Two considerations which have somewhat more bearing on the proposed system are that, in general, the power output of a laser increases with higher doping levels, and that too much energy absorbed in any volume of the rod can cause rod damage. Thus there is a tradeoff between higher power per given rod size and lower doping (and pumping) levels to lengthen rod life. For the Argus and Shiva laser systems, Lawrence Livermore Laboratory has determined that a combination of a special multi-elliptical pump cavity and a constant rod diameter (D)-doping

(P) product of

$$DP = 4\%\text{-cm}$$

gives a uniform beam profile from Nd:silicate glass rods.[16] The LLL experience will be useful when deciding on the best doping level for maximum power with good efficiency in the envisioned Nd:phosphate glass amplifier rods.

For Nd:YAG rods the neodymium doping is usually limited to a maximum of 0.727 to 1%. When doping levels are higher than this the transition lifetime tends to shorten and the linewidth broaden. Also the higher concentration of neodymium causes stresses in the YAG degrading the optical quality. Within these limits the doping level is determined by the application of the laser. Lower doping levels of around 0.5% are used when the laser will be cw, while higher levels (0.87%) are used for Q-switched lasers. As with glass rods the higher doping gives more energy storage at the price of a less uniform beam. The mode locking of the proposed system has a similar effect to Q-switching in that the peak power is increased, and since it is a high power system, so a high doping level will probably be acceptable.[17]

REFERENCES

1. Siegman, A. E., An Introduction to Lasers and Masses, McGraw-Hill New York, 1971, p. 222.

2. Verdeyen, J. T., Laser Electronics, Prentice-Hall, Inc., New Jersey, 1981, p. 225.

3. Koechner, W., Solid-State Laser Engineering, Springer-Verlag, New York, 1976, pp. 457-458.

4. Ibid., p. 476.

5. Ibid., p. 476.

6. Kuizenga, D. J. and Siegman, A. E., "FM and AM Mode Locking of the Homogeneous Laser - Part I: Theory," IEEE J. of Quantum Electronics, QE-6, 11, 1976, p. 696.

7. Kochner, p. 476.

8. Cohen, M. Private communication

9. Koechner, p. 398.

10. Seigman, p. 190.

11. Kuizeya, D. J., Phillion, D. W., Lund, T., Seigman, A. E., "Simultaneous Q-Switching and Mode-Locking in the CW Nd:YAG Laser," Optics Communications, 9, 3, 1973, p. 221.

12. Cohen, M. G., "Continuous-Wave Mode Locked Nd:YAG Lasers: A Picosecord Pump Source for the Future," SPIE, 322, 1982, p. 44.

13. Kuizenga, Phillion, et. al., p. 223.

14. Ibid., p. 221.

15. Schwalby, A., private communication.

16. Lawrence Livermore Laboratory, 1975 Annual Progress Report, p. 144.

17. Koechner, pp. 58-59.

APPENDIX B

THERMAL EFFECTS IN LASER RODS

Heat Generation in the Rods

When a laser system is run either cw or with a high average power, beam distortions caused by thermal effects become a significant problem. These effects are termed thermal lensing and thermal birefringence, both of which will be discussed in greater detail later. The effects occur because of heat generation in the rod, and may be a result of heating during the pumping cycle or of a combination of heating and cooling of the rod. The way thermal effects manifest themselves is dependent on the mode of operation of the rod and the method of cooling.

The heat is generated in the rod by three mechanisms:[1]

1. the transition between the pump bands and the upper level of the laser transition is a radiationless transition in which energy is lost to the host through phonons;
2. the quantum efficiency of the lasing transition is less than unity, meaning some of the energy is lost to the host;
3. the host material directly absorbs pump radiation in the ultraviolet and infared.

The first two mechanisms are grouped together by some authors under the quantum efficiency or the quantum defect.[2] Little can be done to affect them, and they will not be discussed further here.

Operation of the third mechanism is dependent on both the host material and the method of cooling used. Infared absorption by the rod is greatly decreased in systems with water-based coolant because of the

high absorption of infared radiation by the coolant. [3] Some ultraviolet radiation is absorbed by the coolant, which results in deterioration of the coolant, however absorption of radiation by the ultraviolet edge of the host causes a significant heat problem. The ultraviolet edge is the region where the absorptivity of the material increases sharply with decreasing wavelength. [4] In most glasses the ultraviolet edge occurs in the region between 200 and 400 nm. [5] In YAG the edge occurs toward shorter wavelengths and presents less of an absorption problem. Figure 1(a) and Figure 1(b) show a typical Nd^{3+} absorption spectrum in glass with and without the ultraviolet edge. [6]

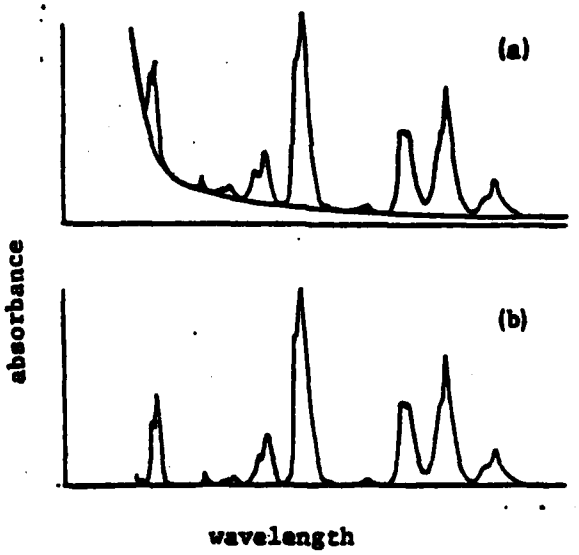

Fig. 1 Absorption spectrum (optical density) of Nd^{3+} in glass in the 200 to 1000 nm region. (a) Baseline is marked. (b) Net Nd^{3+} absorbance after subtraction of the baseline.

In phosphate glasses, as compared to silicate glasses, the ultraviolet edge is shifted towards shorter wavelengths. This results in less absorption because there is less pump energy at the shorter wavelengths.[7] Ultraviolet absorption is particularly bad because the ultraviolet light is absorbed in a very short distance (~nm), causing severe stress in the rod.

Parameters Influencing Thermal Effects

The optical and mechanical response of a laser rod to heating is based on the mechanical and thermal properties of the host material. The following is a list of properties taken from BROWN[8] important in describing thermal effects:

Thermal Properties

K	Thermal conductivity, important in considering the ability of a host (in this case glass or YAG) to dissipate heat, [cal/cm s°C].
c	Specific heat, partially determines the ability of a host to dissipate heat and induced temperature change for unit heat input, [cal/g °C].
α	Thermal-expansion coefficient, partially determines the change of linear index with temperature change, important in determining the curvature in an active-mirror amplifier induced by Xe flashlamp pumping, [$°C^{-1}$].
K/dc	Thermal diffusivity, d is host density [g/cm^3], determines the thermal decay time constant or heat removal time, [cm^2/s].

Mechanical Properties

E	Young's modulus, determines the stiffness of a laser disk or rod, related to host hardness and photoelastic constants, [kg/cm^2].
ν	Poisson's ratio, needed to calculate photoelastic constants, dimensionless.
d	Density, needed to evaluate K/dc, partially determines the induced temperature change for a given heat input, [g/cm^3].
H	Knoop Hardness, determines the abrasion resistance of a host, directly related to rupture strength [kg/cm^2].

Thermal-Optic and Elasto-Optic Properties

$\beta = \frac{dn}{dT}$	Refractive-index temperature coefficient, partially determines the change of linear index with induced temperature change, [$°C^{-1}$].
$\beta+\alpha(n-1)$	Thermo-optic coefficient, in the absence of stress in a host gives the total change of linear index for a given ΔT, [$°C^{-1}$].
B_1, B_{11}	Photoelastic constants, partially determine the change of index or optical pathlength with applied stress in the perpendicular (B_1) or parallel (B_{11}) directions, [(nm/cm)/(kg/cm^2)].
B	Stress-optic coefficient, given by $B = B_1 - B_{11}$, [(nm/cm)/(kg/cm^2)].

There are certain general rules of thumb which apply when comparisons are made between the various properties of YAG, silicate glasses, and phosphate glasses. These are by no means absolute for all varieties of glass, but will give some idea of what to expect. Following BROWN [8] these general relationships are given. For details of properties of specific glasses or YAG, tables such as the Nd-Doped Laser Glass Spectroscopic and Physical Properties [9] should be consulted. YAG, being a

crystal, has a much higher thermal conductivity (K) than the glasses. On the average the thermal conductivity of the phosphate glasses is very much less than that of the silicate glasses. Thus YAG has the highest ability to dissipate heat and the phosphate glasses the lowest. The specific heat (c) of the phosphates and the silicates varies without regard for composition, with the specific heat of YAG falling toward the low end of the range. Thermal expansion (α) tends to be greater for phosphates than for silicates. The thermal expansion of YAG depends on the crystal axis, averaging about the same as the silicates. The higher the thermal expansion, the greater the problem of thermal lensing. Young's modulus (E) and the Knoop Hardness (H) are both much higher for YAG, a crystal, than for the glasses. The phosphate glasses have both the lowest Young's modulus and the lowest hardness. The photoelastic constants, B_r and B_ϕ, are smaller for the silicates than for phosphates, however, the stress-optic coefficient (B) is usually greater for silicate glasses. As a result of this the phosphate glasses tend to suffer less from stress birefringence than silicates, although the silicates generate less heat and cool more quickly.

Thermal Profiles and Optical Distortion Effects

While qualitatively, thermal effects in laser rods are always the same, the manifestation of those effects varies according to the amount and the distribution of heat in the rod. Thermal profiles and corresponding thermal effects will be discussed below for different operating conditions. Much of the notation used will follow KOECHNER (Solid-State Laser Engineering) [10] as will some of the organization.

The three basic modes of operation of a solid state laser are continuous (cw), single-shot, and repetitively pulsed. [11] The single-shot differs from the repetitively pulsed laser in that the single-shot laser is allowed time to totally thermally relax between shots, whereas the repetitively pulsed laser frequently is not. The behavior of the repetitively pulsed laser approaches that of cw operation or single-shot operation depending on the ratio of the pulse interval to the thermal relaxation time of the host (usually glass for pulsed systems).

The thermal effects produced by heat generated during operation are thermal focusing or lensing, bifocusing, and (stress) birefringence. [12] These are the result of thermally induced stress and/or expansion of the rod which produce: (1) a change in length; (2) a temperature-dependent change in the index of refraction; (3) a stress-related change in the index of refraction. [13]

Considering the simple case of a continuously pumped rod with uniform internal heat generation, cooled by a fluid flowing along the rod surface and ignoring end effects, the steady state heat distribution in the rod is obtained from the heat conduction equation. [14,15]

$$\frac{d^2T}{dr^2} + \frac{1}{r}\frac{dT}{dr} + \frac{Q}{K} = 0$$

where Q = rate of heat generation per unit volume

K = thermal conductivity

Solving this for a rod of radius a with the boundary condition $T(r=a)=T_s$ gives [16]

$$T(r) = T_s + (Q/4K)(a^2 - r^2)$$

Using η as the fraction of electrical power input into the lamp (P_{in}) which is dissipated as heat in the rod (P_a), the temperature distribution in terms of the coolant temperature (T_F) is

$$T(r) = T_F + \frac{\eta Pin}{2\ aLh} + \frac{\eta Pin}{4\ a^2 LK}\ (a^2 - r^2)$$

where h = surface heat transfer coefficient ($W/cm^{2\circ}K$). Note that the temperature profile is quadratic, and that the temperature is highest at the center of the rod.

The higher temperatures at the rod center generate stresses because the center of the rod would tend to expand but is prevented from expanding by the cooler outer portion of the rod. Thus the center of the rod is under compression while the exterior sections are under tension. A graph of the stresses as a function of radius for an Nd:YAG rod is shown in Figure 2. [17]

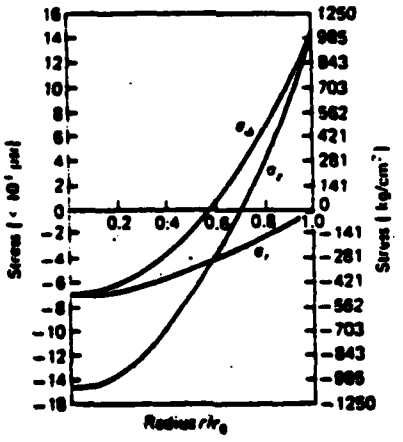

Fig. 2 Radial (σ_r), tangential (σ_ϕ), and axial (σ_z) stress components within a Nd:YAG crystal as a function of radius.

Note that as power dissipation in the rod increases the tension on the outer surface of the rod also increases. For power levels which are too high the tensile strength of the rod material can be exceeded, causing rod fracture.

With a temperature profile available, the stresses in the rod due to thermal causes can be calculated. RIEDEL and BALDWIN give the stress relations for an isotropic material as [18]

$$\sigma_r(r,t) = \frac{\alpha E}{1-\nu}\left[\frac{1}{a^2}\int_0^a T(r,t)\, rdr - \frac{1}{r^2}\int_0^r T(r,t)\, rdr\right]$$

$$\sigma_\theta(r,t) = \frac{\alpha E}{1-\nu}\left[\frac{1}{a^2}\int_0^a T(r,t)\, rdr + \frac{1}{r^2}\int_0^r T(r,t)\, rdr - T(r,t),\right]$$

$$\sigma_z(r,t) = \frac{\alpha E}{1-\nu}\left[\frac{2}{a^2}\int_0^a T(r,t)\, rdr - T(r,t)\right]$$

These hold for laser glasses, which are isotropic materials, and YAG, which, although not isotropic, has elastic behavior very much like an isotropic material. [19] From these relations the thermal stresses for the cw-driven rod are calculated to be. [20]

$$\sigma_r(r) = \frac{\eta P_{in}\alpha E}{16(1-\nu)K\pi L}(r^2 - a^2)$$

$$\sigma_\phi(r) = \frac{\eta P_{in}\alpha E}{16(1-\nu)k\pi L}(3r^2 - a^2)$$

$$\sigma_z(r) = \frac{\eta P_{in} \alpha E}{8(1-\nu) K \pi L} (2r^2 - a^2)$$

The thermal strain distribution can be determined using the stress-strain relationships [21]

$$\varepsilon_r = \frac{1}{E} [\sigma r - \nu(\sigma\phi + \sigma_z)] + \alpha T$$

$$\varepsilon_\phi = \frac{1}{E} [\sigma_\phi - \nu(\sigma_r + \sigma_2)] + \alpha T$$

$$\varepsilon_z = \frac{1}{E} [\sigma_z - \nu(\sigma_r + \sigma_\phi)] + \alpha T$$

The thermal strains for the rod are then [22]

$$\varepsilon_r = \frac{\alpha \eta P_{in}}{16(1-\nu) K R a^2 L} [(3-\nu)a^2 - 3(\nu+1)\ r^2] + \alpha T_s$$

$$\varepsilon_\phi = \frac{\alpha \eta P_{in}}{16(1-\nu) K \pi a^2 L} [(3-\nu)a^2 - (\nu+1)\ r^2] + \alpha T_s$$

$$\varepsilon_z = \frac{\alpha \eta P_{in}}{8 K \pi L} + \alpha T_s$$

Using the calculated strains in combination with the fourth-rank photoelectric tensor, the change in the indicatrix (index ellipsoid or

ellipsoid of wave normals) can be calculated. The indicatrix, described by BORN and WOLF [23] is a mathematical construct whose properties can be used to find the index of refraction for a particular propagation direction or polarization. Changes in the components B_{ij} are given by

$$\Delta B_{ij} = P_{ijkl} c_{kl}$$

With the changes in the indicatrix the changes in the index of refraction for radially and azimuthally (tangentially) polarized light can be calculated. These changes are given by [24]

$$\Delta n_r = \frac{1}{2} n_o^3 \Delta B_r$$

$$\Delta n_\phi = -\frac{1}{2} n_o^3 \Delta B_\phi$$

While YAG may be treated as isotropic elastically, the photoelastic effect in YAG is not isotropic. Because YAG laser rods are grown with the axis in the [1 1 1] direction and the published values are for the [1 0 0] orientation, a transformation must be performed to the [1 1 1] for the ΔB calculation when dealing with YAG. Once the transformation has been performed the changes in the indicies of refraction are [25]

$$\Delta n_r = -\frac{1}{2} n_o^3 \frac{\alpha \Omega P_{in}}{K w a^2 L} C_r r^2$$

$$\Delta n_\phi = -\frac{1}{2} n_o^3 \frac{\alpha n P_{in}}{\kappa \pi a^2 L} C_\phi r^2$$

where

$$C_r = \frac{(17\nu-7)\ P_{11} + (31\nu-17)\ P_{12} + 8(\nu+1)\ P_{44}}{48(\nu-1)}$$

$$C_\phi = \frac{(10\nu-6)\ P_{11} + 2(11\nu-5) P_{12}}{32(\nu-1)}$$

In both Δn_r and Δn_ϕ there is an additional additive constant term which is not shown above. Since only the radial variations are necessary to calculate the thermal focal lengths and the induced birefringence the constant terms may be dropped (see FOSTER and OSTERINK, Ref. 25).

With the thermal profile and the stress distribution in the rod optical effects originating from thermal causes may be examined quantitatively.

Since the index of refraction is changed independently by temperature and by stresses the index of refraction may be written in three parts

$$n(r) = n_o + \Delta n(r)_T + \Delta n(r)_s$$

where n_o = index of refraction at the center of the rod.

Thermal focusing is caused by both the temperature related change and the stress related change in the index of refraction.[26] The major contribution to thermal focusing (~74%) comes from the variation of refractive index with temperature. Another 20% is accounted for by stress related changes in the index of refraction, which also introduce biaxial focusing (different focal lengths for different polarization directions). The remaining 6% of the effect is caused by curvature of the end faces.

That this last portion should be so small is expected because the x-component of the thermal strain distribution has no r dependence, i.e. thermal focusing is not caused by the rod being distorted into a lens shape. [27]

Examining the thermal part of the index of refraction it may be seen from previous expressions that the temperature change radially between the center of the rod and a point a distance r away is

$$\Delta T = - \frac{\eta P i n}{4 K \pi a^2 L} r^2$$

This gives

$$\Delta n(r)_T = - \frac{\eta P i n}{4 K \pi a^2 L} \frac{dn}{dT} r^2$$

With the thermal and stress variations the total refractive index may be written

$$n(r) = no \left[1 - \frac{\eta P i n}{2 K \pi a^2 L} \left(\frac{1}{2 n_o} \frac{dn}{dT} + n_o^2 \alpha C\right) t^2\right]$$

The C represents either the radial (C_r) or the aximuthal (C_ϕ) photoelastic constant, and thus there are different indicies of refraction for the two polarization directions. Note that both the thermal part and the stress related part of the index of refraction have a quadratic radial dependence. For a medium in which the index of refraction has a quadratic variation

$$n(r) = n_o \left(1 - \frac{2}{b^2} r^2\right)$$

the focal length is given by [28]

$$f = \frac{b}{2n_o} [\sin (\frac{2}{b}) L]^{-1}$$

where L is the rod length and b is a constant. Substituting the coefficient of r in the refractive index for b gives

$$f = \frac{\eta Pin}{4n_o K\pi a^2 L} (\frac{1}{2n_o} \frac{dn}{dT} + n_o \alpha C) [\delta_{in} [\frac{\eta_o Pin}{K\pi a^2 L} (\frac{1}{2n_o} \frac{dn}{dT} + n_o^2 \alpha C)]^{-1}\}^{-1}$$

The two possible values of C will give two focal lengths, dependent on polarization direction (biaxial focusing). For a long focal length compared to the rod length $2L/b << 1$ and the focal length is approximately.

$$f = \frac{K\pi a^2}{\eta Pin} [\frac{1}{2} \frac{dn}{dT} + \alpha C n_o^3]^{-1}$$

The end effects can be taken into account by finding the curvature of the rod ends caused by stresses and expansion. The radius of curvature of the ends is [29]

$$R = \frac{2\pi a^2 L}{\eta Pin \alpha a}$$

Using the thick-lens formula [30]

$$f = \frac{R}{2(n_o - 1)}$$

Substituting for R, the expression for the thermal focal length of a cw-pumped rod is

$$f = \frac{K\pi a^2}{\eta P_{in}} \left[\frac{1}{2}\frac{dn}{dT} + \alpha C n_o^3 + \frac{\alpha a(n_o-1)}{L}\right]^{-1}$$

with the biaxial focusing caused by the difference in refractive index for different polarizations.

Note that the same treatment will work for rods which are not cw-driven, however, the temperature profile must be changed to reflect the differnce in operating mode. There will be more on different modes of operation further on in this report.

The third thermal effect, birefringence, is caused by the anisotropy of the photoelectric effect. Because of the anisotropy the radially polarized component of light passing through the rod encounters a different index of refraction than the azimuthally polarized component. The difference in the indicies of refraction can be determined by subtracting the stress induced changes in the total index of refraction for different polarization directions from one another. The induced birefringence for a cw-driven rod is then

$$\Delta n_r - \Delta n_\phi = n_o^3 \frac{3\alpha\eta P_{in}}{K\pi a^2 L} C_B r^2$$

where $C_B = \frac{1+\nu}{48(1-\nu)} (P_{11} - P_{12} + 4P_{44})$

Because of the difference in refractive indicies the phase relationship between the two polarizations will be changed and linearly polarized light passing through the rod will emerge elliptically polarized.

There are three areas in the rod where this will not occur. Two of the areas are along mutually perpendicular axes in the plane perpendicular to the long axis of the rod. Along those axes only one index of refraction exists, n_r for the one axis and n_ϕ for the perpendicular axis. Because of the single index of refraction light traversing the rod along these axes will have no change in the phase relationship between radial and azimuthal polarizations. The third area where no effect will be observed is along concentric circles centered on the rod center where the total induced phase change is equal to an integral multiple of wavelengths. In this case the change is effectively zero because of the cyclic nature of waves.

This effect may be observed by sending an upcollimated beam from a He-Ne laser through the rod between crossed polarizers. Where the polarization is changed, the crossed polarizers will partially transmit the light. The unaffected light will be stopped by the second polarizer. The pattern will show the cross and ring(s) (isogyre) structure described above for the areas unaffected by the birefringence. A copy of a photograph of this structure is shown in Fig. 3. [31]

The reason that thermal birefingence presents a problem is that several aspects of laser operation depend on a linearly polarized beam to work. The polarized beam is supplied by putting a polarizer in the cavity. The in-cavity polarizer linearly polarizes the beam, which then is partially depolarized by thermal birefringence. The portion of the depolarized beam orthogonal to the axis of the polarizer is then removed by the polarizer. This occurs each round trip in the cavity until the beam is emitted. The birefringence also deforms the beam in the process of depolarizing it.

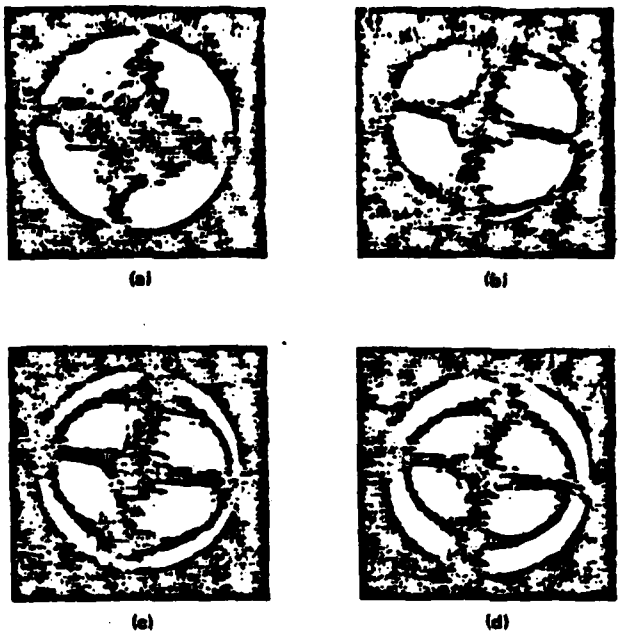

Fig. 3. Thermal stresses in a 7.5-cm-long and 0.63-cm-diameter Nd:LaSOAP crystal. The rod was pumped at a repetition rate of 40 pps by a single xenon flashlamp in an elliptical pump cavity. Input power (a) 115 W, (b) 450 W, (c) 590 W, (d) 880 W.

To calculate light transmitted observe that to light circulating in the cavity the rod and polarizer are the same as a rod twice as long between two parallel polarizers. BORN and WOLF give the fraction of transmitted intensity as [32]

$$\frac{I_{out}}{I_{in}} = 1 - \sin^2(2\phi)\sin(\frac{\delta}{2})$$

where ϕ = angle between the polarizer and one of the principal birefringence axes

δ = polarization phase shift

For the cw-pumped rod the single-pass phase difference is [33]

$$\delta = \frac{2\pi}{\lambda} L (\Delta n_\phi - \Delta n_r) = \frac{n_o^3 \alpha \eta P_{in}}{K \pi a^2 L} C_B r^2$$

Since the birefringence is not constant integration over the area of the rod is required to find the total fractional transmitted intensity. This has been done for the multimode case by KOECHNER [34] and by KARR [35] and for the TEM case by KARR [36]. For the multimode case the integral is

$$\frac{I_{out}}{I_{in}} = \frac{1}{\pi a^2} \int_o^{2\pi} \int_o^a (1 - \mathrm{Sin}^2 2\phi \, \mathrm{Sin}^2 \tfrac{\delta}{2}) \, r dr d\phi$$

with a fractional transmission of

$$\frac{I_{out}}{I_{in}} = \frac{3}{4} + \frac{\mathrm{Sin}\,(2 n_o^3 \alpha \eta P_{in} C_B/\lambda K)}{8 n_o^3 \alpha \eta \, P_{in} C_B/\lambda K}$$

For the TEM case the integral is

$$\frac{I_{out}}{I_{in}} = \frac{1}{\pi a^2} \int_o^{2\pi} \int_o^a e^{\frac{-2r^2}{w^2}} (1 - \mathrm{Sin}^2 2\phi \, \mathrm{Sin}^2 \tfrac{\delta}{2}) \, r dr d\phi$$

with a fractional transmission of

$$\frac{I_{out}}{I_{in}} 1 - \frac{(n^3_o \alpha\eta \text{ Pin } C_B/\lambda K)^2}{64 + 4(n^3_o \alpha\eta \text{Pin} C_B/\lambda K)^2}$$

The extra term $e^{\frac{-2r^2}{w^2}}$ is an amplitude profile term with w being the radius of the beam. If the rod length is small compared to the mirror radius w may be treated as a constant. Cavity losses can be determined by subtracting the fractional transmission from one. A graph of cavity losses verses pumping power for multimode and TEM is shown in Fig. 4.

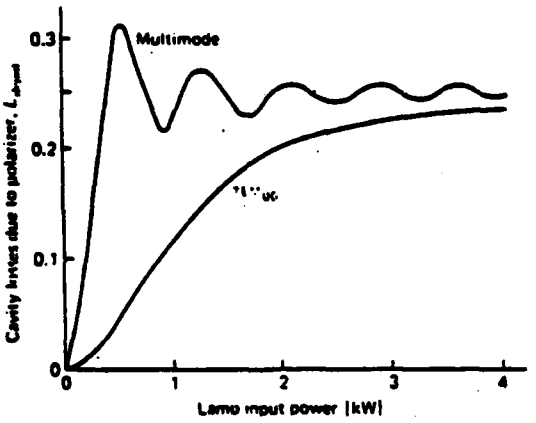

Fig. 4. Calculated resonator loss caused by the combination of thermally induced birefringence in a Nd:YAG rod and an intracavity polarizer.

The TEM losses are smaller because the beam is confined closer to the center of the rod where the induced birefringence is less. [37]

Single-shot operation is characterized by a (fast) pump pulse followed by a period of cooling long enough for the rod to lose the heat gained from the pulse. Thermal effects during single-shot operation

depend on the uniformity of the absorption of pump radiation. Because lasing occurs at or near the end of the pump pulse, cooling does not affect the temperature of the rod during the time when light is passing through it. The thermal profile of the rod is thus determined by the absorption of the pump pulse in the rod. For uniform absorption the temperature in the rod is constant throughout the rod (for the period of light transmission). In this case the thermal effects are limited to a frequency shift of the laser radiation and an increase of the optical path length caused by linear thermal expansion and by the change in index of refraction with change in temperature. KOECHNER [38] gives the optical path length change as

$$\Delta(\text{o.p.l.}) = \frac{dn}{dT} L + n_o L \alpha \Delta T$$

Some work has been done on the problem of finding the thermal profile of a pulse-pumped rod, however most of the solutions were based on the assumption that the surface temperature remained constant when in fact the coolant temperature remained constant and the rod surface temperature varied. [39] The results using the constant surface temperature assumption yielded thermal relaxation times which were two to three times shorter than those observed experimentally. In a 1973 paper KOECHNER [40] did a treatment of the thermal profile of a pulse pumped rod for the general case. It was assumed that any pumping nonuniformity could be treated as a parabolic function. Using this the temperature distribution at the end of pumping is

$$T(r, o) = \Delta T \left[1 + g\left(\frac{r}{a}\right)^2\right]$$

where ΔT is the temperature rise at the center of the rod and g is a pumping uniformity factor: $g = 0$ uniform pump distribution, $g > 0$ more pumping at the rod surface, $g < 0$ more pumping at the rod center.

As described above, for the uniform pumping case the effect will be an increase in the optical path length. For the $g < 0$ case there will be a converging lens effect, as calculated for the cw-driven rod. When $g < 0$ a diverging lens effect will be seen.

For a repetitively pumped rod the situation varies with the repitition rate from the single-shot case to the cw case. The critical parameter in determining how thermal effects will affect the rod is the ratio of the time between pulses to the thermal time constant of the rod. The thermal time constant is [41]

$$\tau = \frac{a^2}{K}$$

where K is the thermal diffusivity defined above. The thermal relaxation time, defined as the time for the temperature jump to drop to 1/e of its initial value, is [42]

$$\tau' = \frac{a^2}{4k}$$

KOECHNER [40] has developed an expression for the temperature profile in a repetitively pulsed rod. His result is

$$T(r,t) = 2\Delta T \sum_{n=1}^{\infty} \exp\left[-\frac{\beta_n^2 t\, J_o(\beta n\, r/a)}{\tau\,(A^2+\beta_n^2)J_o^2(\beta_n)}\right]\left[(1+g)\beta n J_1(\beta_n) - 2gJ_2(\beta)\right]$$

$$\times\left[\frac{1-\exp(-M\beta_n^2\, tp/\tau)}{1-\exp(-\beta_n^2\, tp/\tau)}\right]$$

where M = number of shots

t_p = pulse interval

τ = thermal time constant

A = ah/K: cooling condition of the rod

β_n = roots of $\beta_n J_1(\beta_n) = AJ_o(\beta_n)$

Figure 5 shows the relationship of temperature build-up to thermal relaxation ratio.[43]

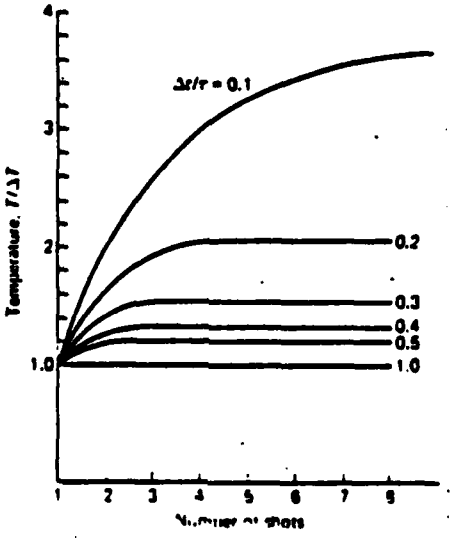

Fig. 5. Temperature buildup in the center of a repetitively pumped laser rod versus number of shots. Parameter is the normalized repetition rate. Cooling factor A = 10, pumping coefficient g = 0.

With the thermal profile the thermal effects can be calculated in the same manner as for the cw-pumped case. Thermal lensing as a function of repetition rate is shown in Fig. 6.[44]

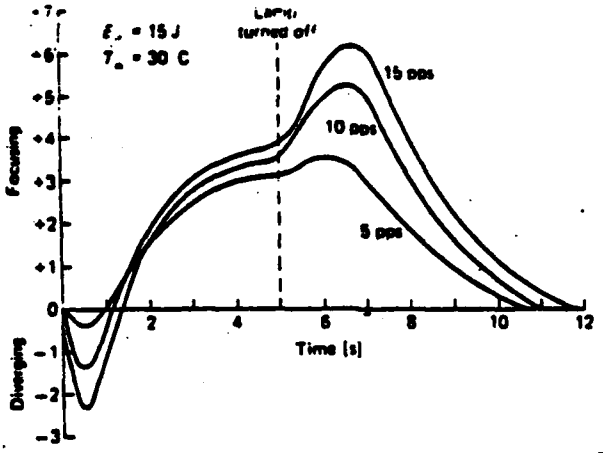

Fig. 6. Thermal lensing in a Nd:YAG laser rod as a function of repetition rate.

REFERENCES

1. Koechner, W., Solid State Laser Engineering, Springer-Verlag, New York, 1976, p. 344.

2. Brown, D. C., High Peak Power Nd:Glass Laser Systems, Springer-Verlag, New York, 1981, p.83.

3. Koechner, W., Solid State Laser Engineering, Springer-Verlag, New York, 1976, pp. 366, 382.

4. Brown, D. C., High Peak Power Nd:Glass Laser Systems, Springer-Verlag, New York, 1981, p.3.

5. Stokowski, S. E., Saroyan, R. A. and Weber, M. J., Nd-Doped Laser Glass Spectroscopic and Physical Properties, Lawrence Livermore Laboratory, Livermore, CA, 1981, p.6.

6. Stokowski, S. E., Saroyan, R. A., and Weber, M. J., Nd-Doped Laser Glass Spectroscopic and Physical Properties, Lawrence Livermore Laboratory, Livermore, CA, 1981, p. 6.

7. Brown, D. C., High Peak Power Nd:Glass Laser Systems, Springer-Verlag, New York, 1981, p. 84.

8. Brown, D. C., High Peak Power Nd:Glass Laser Systems, Springer-Verlag, New York, 1981, p. 72.

9. Stokowski, S. E., Saroyan, R. A., and Weber, M. J., Nd-Doped Laser Glass Spectroscopic and Physical Properties, Lawrence Livermore Laboratory, Livermore, CA, 1981.

10. Koechner, W. , Solid State Laser Engineering, Springer-Verlag, New York, 1976.

11. Koechner, W., Solid State Laser Engineering, Springer-Verlag, New York, 1976, Chapter 7.

12. Foster, J. D. and Osterink, L. M., "Thermal Effects in a Nd:YAG Laser," Journal of Applied Physics, 41, 9, 1970, p. 3656.

13. Baldwin, G. D. and Riedel, E. P., "Measurements of Dynamic Optical Distortion in Nd-Doped Glass Laser Rods," Journal of Applied Physics, 38, 7, 1967, p. 2720.

14. Carslaw, H. S. and Jaeger, J. C., Conduction of Heat in Solids, Oxford University Press, London, 1948, p. 191.

15. Churchill, R. V. and Brown, J. W., Fourier Series and Boundary Value Problems, McGraw-Hill, New York, 1978, p. 207.

16. Foster, J. D. and Osterink, L. M., "Thermal Effects in a Nd:YAG Laser," Journal of Applied Physics, 41, 9, 1970, p. 3657.

17. Koechner, W., "Absorbed Pump Power, Thermal Profile and Stresses in a CW Pumped Nd:YAG Crystal," Applied Optics, 9, 6, 1970, p. 1433.

18. Riedel, E. P., and Baldwin, G. D., "Theory of Dynamic Optical Distortion in Isotropic Laser Materials," Journal of Applied Physics, 38, 7, 1967, p. 2720.

19. Foster, J. D. and Osterink, L. M., "Thermal Effects in a Nd:YAG Laser," Journal of Applied Physics, 41, 9, 1970, p. 3657.

20. Koechner, W., "Absorbed Pump Power, Thermal Profile and Stresses in a CW Pumped Nd:YAG Crystal," Applied Optics, 9, 6, 1980, p. 1433.

21. Foster, J. D. and Osterink, L. M., "Thermal Effects in a Nd:YAG Laser," Journal of Applied Physics, 41, 9, 1970, p. 3602.

22. Foster, J. D. and Osterink, L. M., "Thermal Effects in a Nd:YAG Laser," Journal of Applied Physics, 41, 9, 1970, p. 3602.

23. Born, M. and Wolf, E., Principles of Optics, Pergammon Press, New York, 1965, p. 673.

24. Koechner, W., Solid State Laser Engineering, Springer-Verlag, New York, 1976, p. 350.

25. Foster, J. D. and Osterink, L. M., "Thermal Effects in a Nd:YAG Laser," Journal of Applied Physics, 41, 9, 1970, p. 3658.

26. Koechner, W., "Thermal Lensing in a Nd:YAG Laser Rod," Applied Optics, 9, 11, 1970, p. 2548.

27. Foster, J. D. and Osterink, L. M., "Thermal Effects in a Nd:YAG Laser," Journal of Applied Physics, 41, 9, 1970, p. 3657.

28. Foster, J. D. and Osterink, L. M., "Thermal Effects in a Nd:YAG Laser, Journal of Applied Physics, 41, 9, 1970, p. 3658.

29. Koechner, W., Solid State Laser Engineering, Springer-Verlag, New York, 1976, p. 353.

30. Hecht, E. and Zajac, A., Optics, Addison-Wesley, Reading, MA, 1975, p. 168.

31. Koechner, W., Solid State Laser Engineering, Springer-Verlag, New York, 1976, p. 358.

32. Born, M. and Wolf, E., Principles of Optics, Pergammon Press, New York, 1965, p. 695.

33. Koechner, W., Solid State Laser Engineering, Springer-Verlag, New York, 1976, p. 358.

34. Koechner, W., Solid State Laser Engineering, Springer-Verlag, New York, 1976, p. 359.

35. Karr, M. A., "Nd:YAlG Laser Cavity Loss Due to CM an Internal Brewster Polarizer," Applied Optics, 10, 4, 1971, p. 893.

36. Karr, M. A., "Nd:YAlG Laser Cavity Loss Due to CM an Internal Brewster Polarizer," Applied Optics, 10, 4, 1971, p. 894.

37. Karr, M. A., "Nd:YAlG Laser Cavity Loss Due to CM an Internal Brewster Polarizer," Applied Optics, 10, 4, 1971, p. 894.

38. Koechner, W., Solid State Laser Engineering, Springer-Verlag, New York, 1976, p. 367.

39. Koechner, W., "Transient Thermal Profile in Optically Pumped Laser Rods," Journal of Applied Physics, 44, 7, 1973, p. 3162.

40. Koechner, W., "Transient Thermal Profile in Optically Pumped Laser Rods," Journal of Applied Physics, 44, 7, 1973.

41. Koechner, W., Solid State Laser Engineering, Springer-Verlag, New York, 1976, p. 372.

42. Koechner, W., Solid State Laser Engineering, Springer-Verlag, New York, 1976, p. 374.

43. Koechner, W., "Transient Thermal Profile in Optically Pumped Laser Rods," Journal of Applied Physics, 44, 7, 1973, p. 3164.

44. Koechner, W., Solid State Laser Engineering, Springer-Verlag, New York, 1976, p. 380.

APPENDIX C

REVISED BUDGET

EQUIPMENT COMPONENTS AND COST ESTIMATES

First Year (Items needed to accomplish initial system milestone demonstrating 10 ms. run time and frequency doubling characteristic)

Catagory/Components	Vendor	Price/Delivery ARO
1. Nd:YAG Oscillator, Mode-locked, Q-Switched		
Quantronix Model 116R-Q/ML-QS	Quantronix Corp. 225 Engineers Road Smithtown, NY 11788 (516) 273-6900	$45,000** 3-4 Months
2. Nd:Glass Amplifier #1, 12" x 3/8" pumped, modified for 10 ms pulse train, with controller, w/o rod		
Apollo Cat. No. 26520-S	Apollo Lasers, Inc. 9201 Independence Avenue Chatsworth, CA 91311 (213) 709-1111	$44,000** $46,700 3-4 Months

REVISED BUDGET

EQUIPMENT COMPONENTS AND COST ESTIMATES

Catagory/Components	Vendor	Price/Delivery ARO
Cooling Unit for Amplifier System 1705 BTU/hr. RTE - 8	NESLAB Instruments Inc. P.O. Box 1178 Portsmouth, NH 03801 (603) 436-9444	$ 1,525 1 month
3. High Speed Oscilloscope (1 GHz)		
Mainframe Tektronix 7104, w/o plug-ins	Tektronix Inc. 450 Sentry Parkway Blue Bell, PA 19422 (215) 825-6400 x 514	$20,865 4 1/2 months
Amplifier Tektronix 7A29	Tektronix Inc.	$ 2,620 2 1/2 months
Timebase Tektronix 7B10	Tektronix Inc.	$ 2,185 4 months
Fast Probe Tektronix P6056	Tektronix Inc.	$ 155 3 weeks
C-31 Camera adaptor Tektronix 016-0248-01	Tektronix Inc.	$ 80 1 month

REVISED BUDGET

EQUIPMENT COMPONENTS AND COST ESTIMATES

Catagory/Components	Vendor	Price/Delivery ARO
4. Frequency Altering Crystals		
Second Harmonic Generating KD*P Type II Crystal 25 x 25 x 30 mm & Fluid Cell #532-250 (2 each)	Interactive Radiation Inc. (Inrad) 181 Legrand Avenue Northvale, NJ 07647 (210) 767-1910	$ 4,390 1 1/2 - 2 months
5. Optical Components		
Nd:Glass laser rods 15" x 3/8" for Amplifier #1 LG (3 each) 3.5%, 6° end	Schott Optical Glass Inc. 400 York Avenue Duryea, PA 18642 (717) 457-7485	$ 2,240** 2 1/2 - 3 months
Beam Expander 10x, Oscillator to Amplifier #1 Special Optics 5225-10X-1.06	Special Optics P.O. Box 163, 101 E. Main Street Little Falls, NJ 07424 (201) 785-4015	$ 1,025 1 week
Optical Table-Top 4' x 6' KT-46	Newport Research Corp. 18235 Mt. Baldy Circle Fountain Valley, CA 92708 (714) 963-9811	$ 2,260 1 - 3 weeks

REVISED BUDGET

EQUIPMENT COMPONENTS AND COST ESTIMATES

Catagory/Component	Vendor	Price/Delivery ARO
High Voltage Power Supply Model 1570	Power Designs Inc. 1700 Shames Drive Westbury, NY 11590 (516) 333-6200	$ 695 1 - 2 weeks
Fast Detector for 1.06μ - 40 ps risetime BNC package L-4501 (3 each)	Ford Aerospace and Communications Corp. Ford Road Newport Beach, CA 92663 (714) 759-5851	$ 1,113 1 month
Electronics for detector for 1.06μ Monitor T or Bias T .1-500 GHz HW-02B (3 each)	Microlab FXR 10 Microlab Road Livingston, NJ 07039 (201) 992-7700	$ 300 1 1/2 months
Amplifier for Detector for 1.06μ 2-500 MHz, 1W ZHL-1A (3 each)	M. Lader Company Inc. 456 Germantown Pike Lafayette Hill, PA 19444 (215) 825-3177	$ 597 2 weeks
Miscellaneous (Safety, lenses, alignment lasers)		$ 946
6. Facility Development		$10,000
	Subtotal for first year/initial milestones	$140,000
	less matching University funds (25%)	49,000
	Amount requested (first year)	$ 91,000

** Items to be procured with DOD funds

APPENDIX D

SCHEMATIC OF ND-GLASS MODE LOCKED SYSTEM

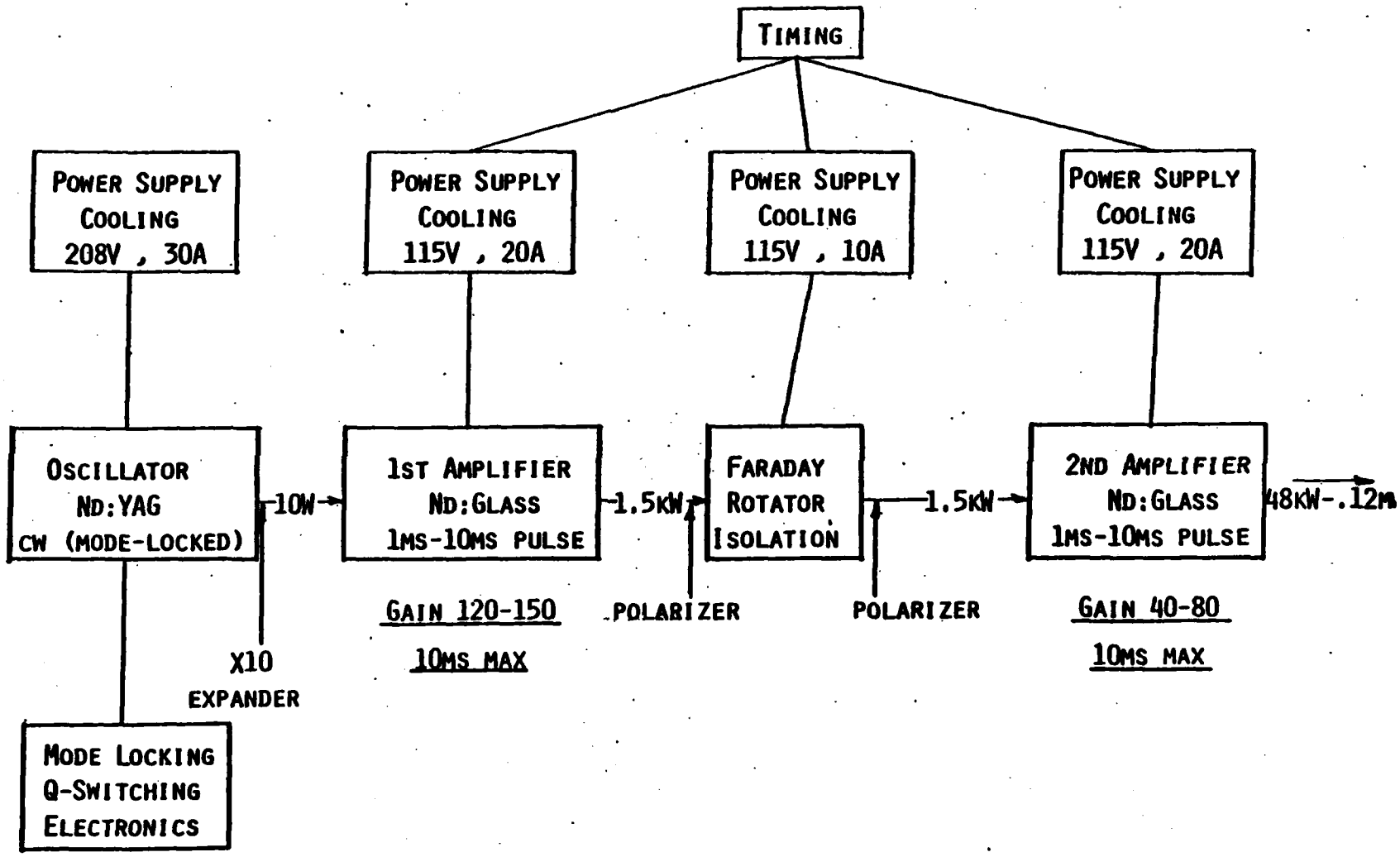

LASER POWER CAPABILITIES AND CHARACTERISTIC TIMES

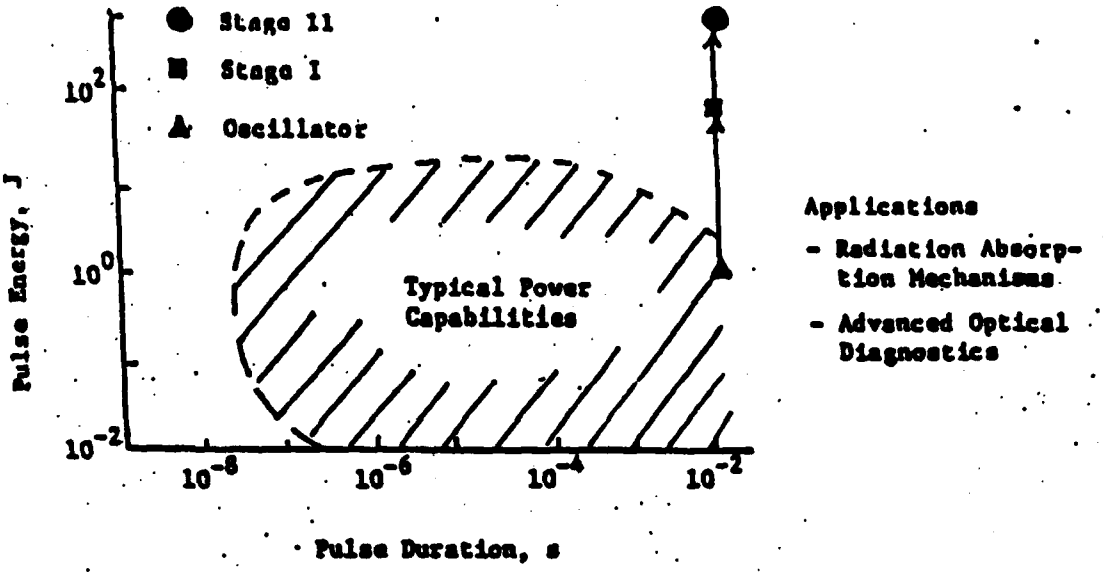

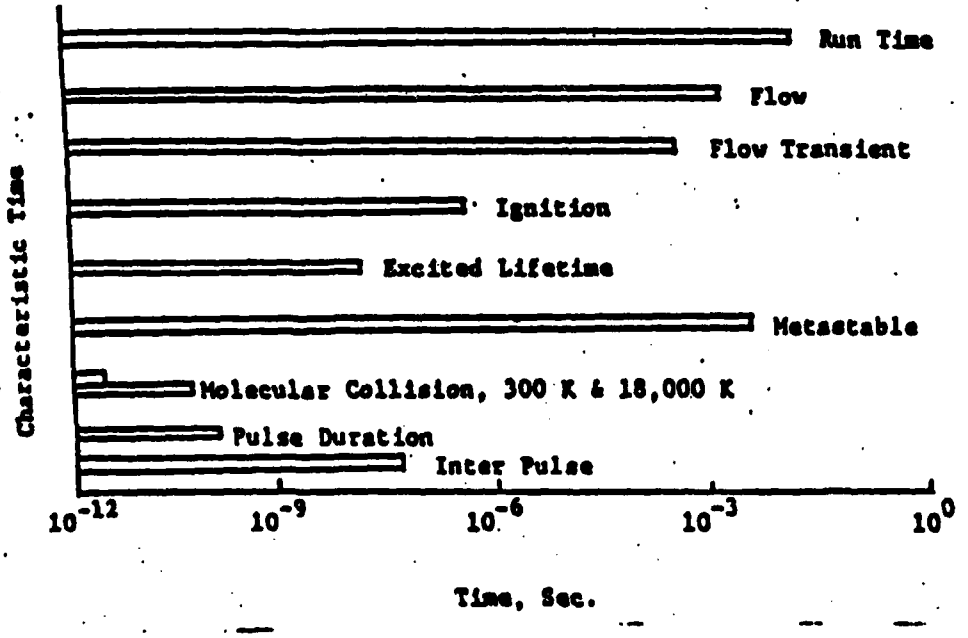

QUANTRONIX MODEL 116 OSCILLATOR

ND-YAG (3MM X 76MM)

OUTPUT APERTURE (TEM_{00}) = 0.6 MM DIA

CW POWER 14 W

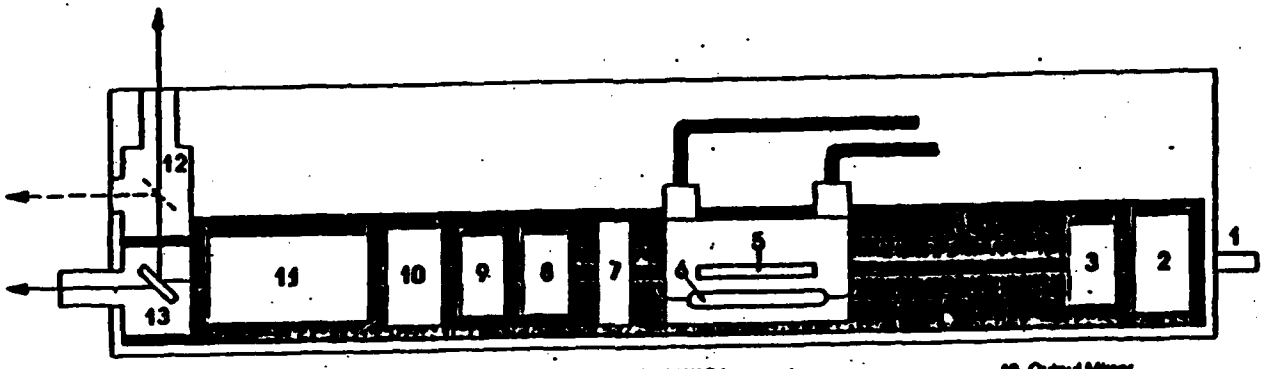

1. Optional Differential Micrometer cavity length adjuster
2. High-reflecting rear mirror
3. Optional Q-Switch
4. Rail with optional Super-Invar Stabilization
5. Nd:YAG laser rod
6. Krypton arc lamp
7. Mode selection aperture
8. Polarizer/Shutter
9. Optional Mode-lock Modulator
10. Output Mirror
11. Optional Second Harmonic Generator
12. Optional 532 nm Beam Splitter
13. Harmonic Separator

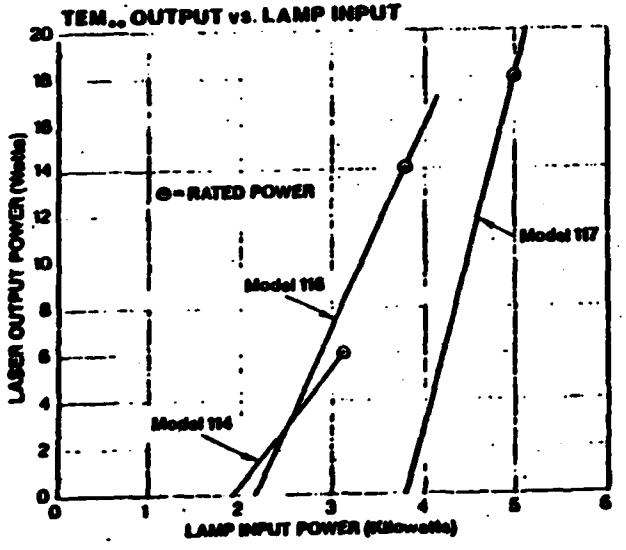

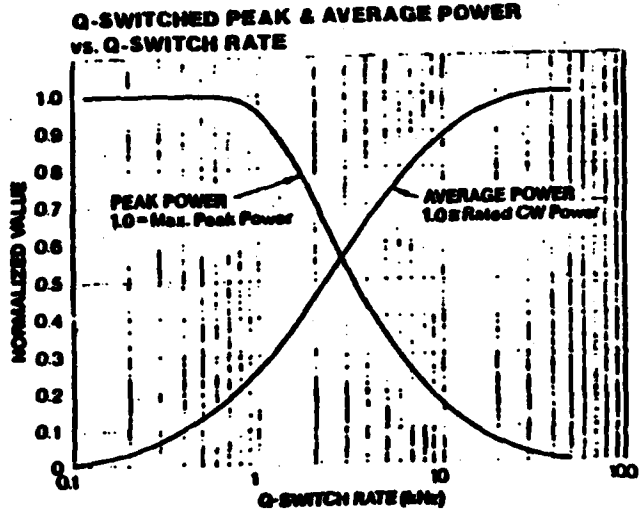

OSCILLATOR PERFORMANCE

CW OPERATION W/WO MODELOCKING

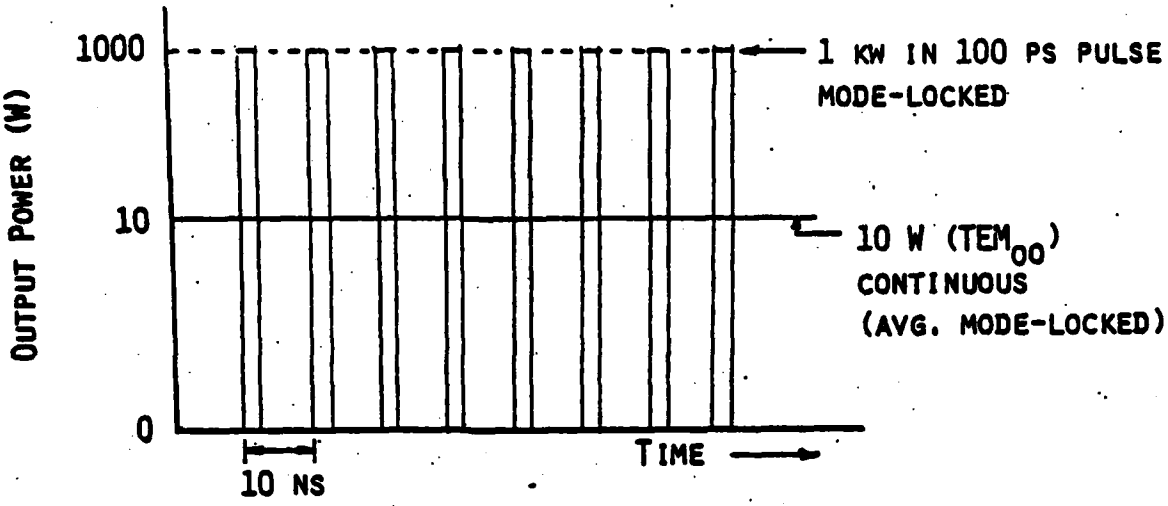

REPETITIVELY Q-SWITCHED OPERATION (WO MODE-LOCKING)

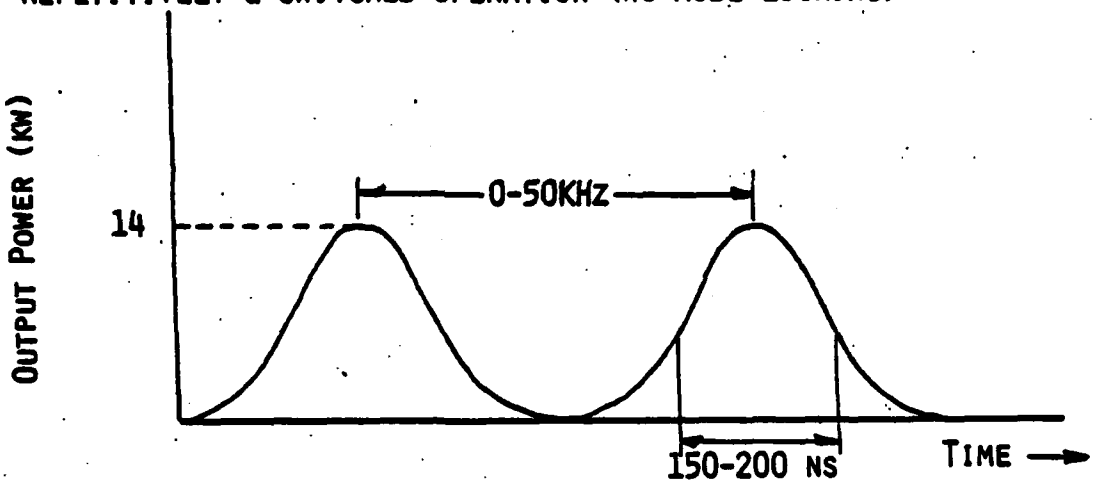

Q-SWITCHED OPERATION WO MODE-LOCKING

Q-SWITCH REP RATE	BURST WIDTH	ENERGY/BURST	AVG POWER	PEAK POWER
500Hz	150ns	2mJ	1.5w	14kw
2KHz	170ns	1.4mJ	5.1w	9.8kw
5KHz	200ns	0.7mJ	7.6w	4.9kw

AMPLIFIER CHARACTERISTICS

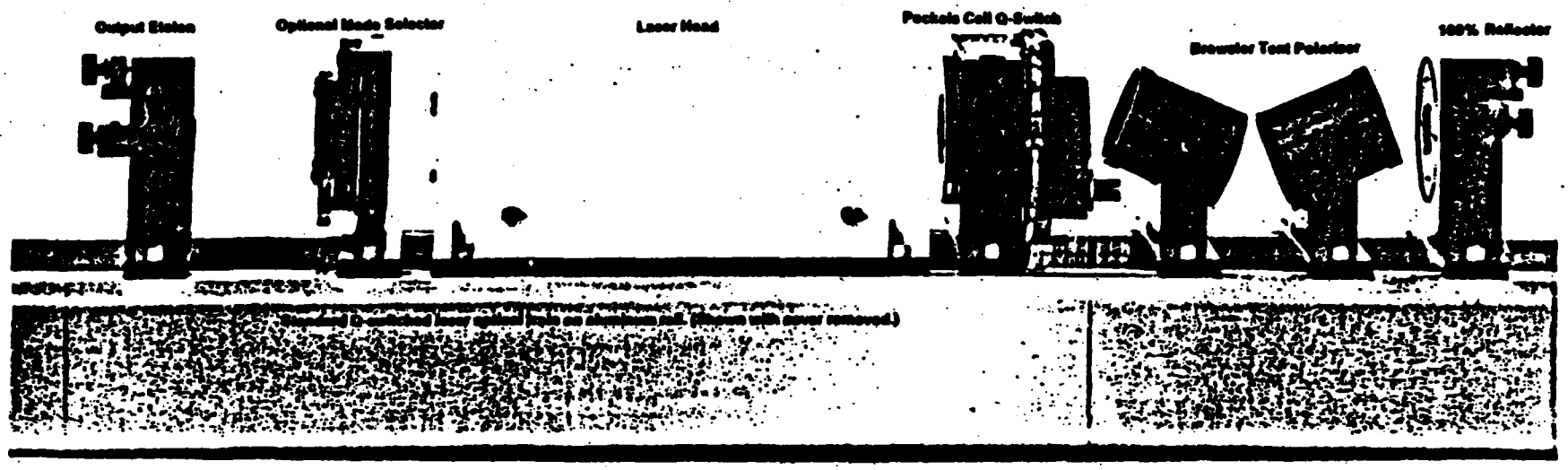

AMPLIFIER #1: APOLLO MODEL 26520-S 12" X 3/8" ROD ND-GLASS #1 GAIN : 120-150

AMPLIFIER #2: APOLLO MODEL 26520-S 12" X 3/8" ROD ND-GLASS #2 GAIN 40-80

REQUIREMENTS:

1. PRECISE CONTROL OF BEAM UNIFORMITY (POWER FLUX NEAR DAMAGE THRESHOLD)
2. EVALUATION OF BEAM AMPLIFICATION GAIN, ESP. WITH 0-5KHZ OPERATION
3. INTERSTAGE ISOLATION TO CONTROL AMPLIFIER STAGING

   FARADAY ROTATION ISOLATER BETWEEN 1ST AND 2ND STAGES

System Performance

	Modelocked			Q-Switched (150 ns Burst)	
	Average Power 10ms Run Time	Peak Power per 100ps Modelocked Pulse	Energy per 100ps Modelocked Pulse	Peak Power/ Burst	Energy/ Burst
Oscillator →	10W	1KW	100nJ	14KW	2-2.5mJ
1st Amplifier → (Gain 120)	1.2KW	.12MW	12μJ	.15MW (EST)	20mJ (EST)
2nd Amplifier → (Gain 65)	80KW	8MW	0.8mJ	0.7MW (EST)	100mJ (EST)

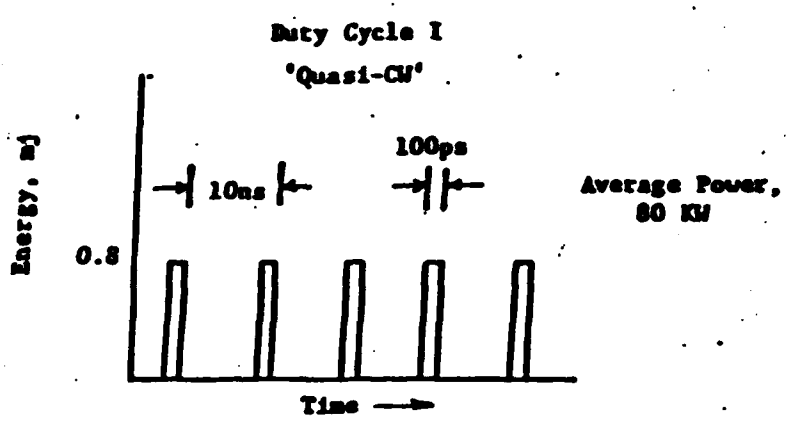

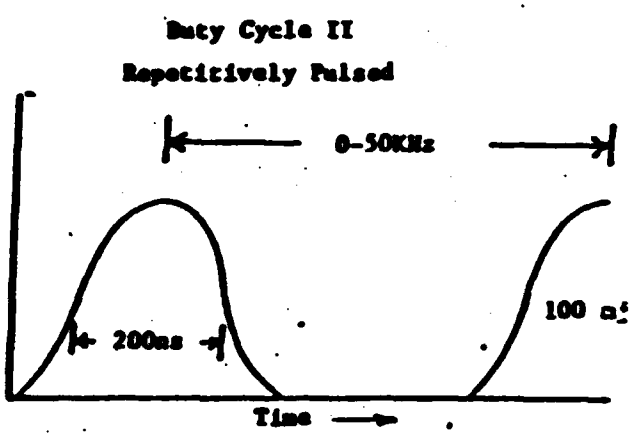

APPENDIX E

I. LASER OUTPUT

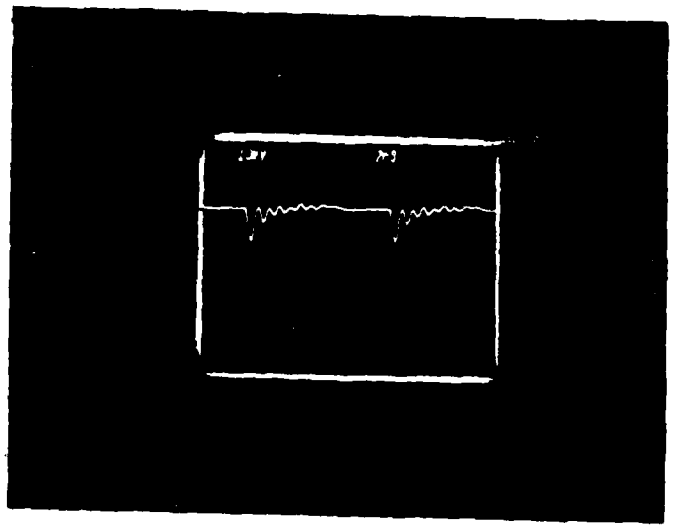

Mode-Locked Pulses
(oscillator)

Horiz.: 2 ns/DIV

Vert.: 10 mV/DIV

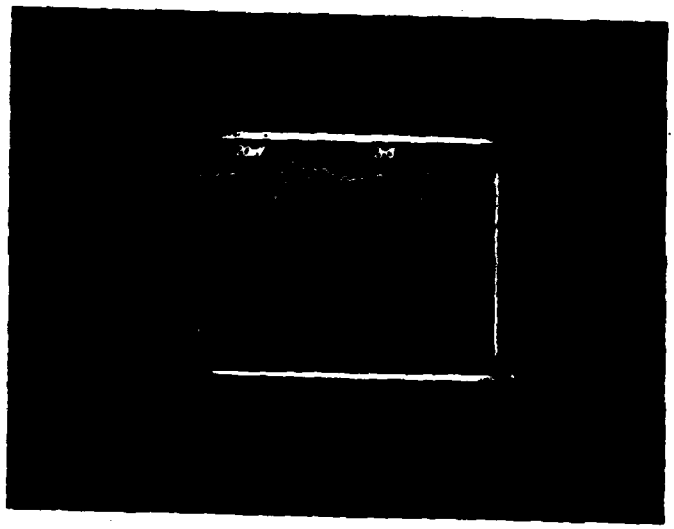

Amplified Mode-Locked
Pulses

Flashlamp: 4.9kV

Horiz.: 2 ns/DIV

Vert.: 20 mV/DIV (filtered)

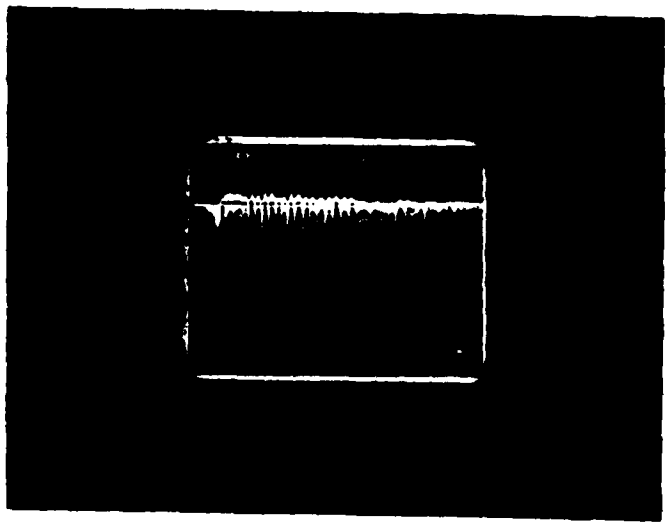

Amplified Mode-Locked 10ms Burst

Flashlamp: 4.9kV

Horiz.: 1 ns/DIV

II. Flashlamp Current and Voltage Records

(10 capacitor/loop)

Flashlamp A

470 A /div (Ragowski Loop)

2000 V/div (Voltage Probe)

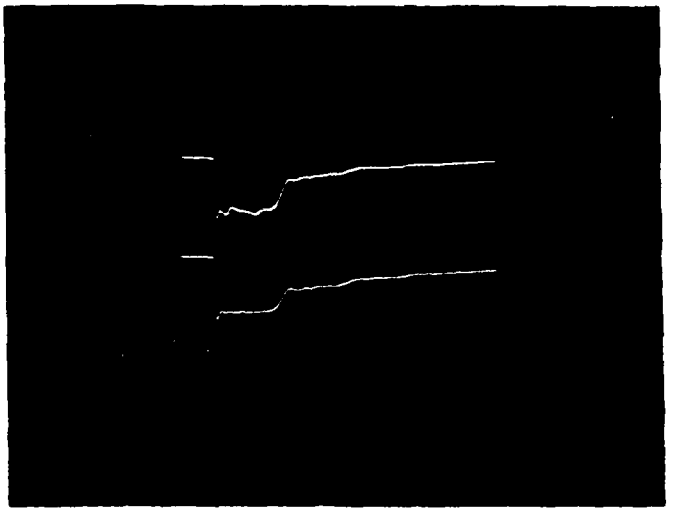

5 ms/div

Flashlamp B

470 A /div (Ragowski Loop)

200 V/div (Voltage Probe)

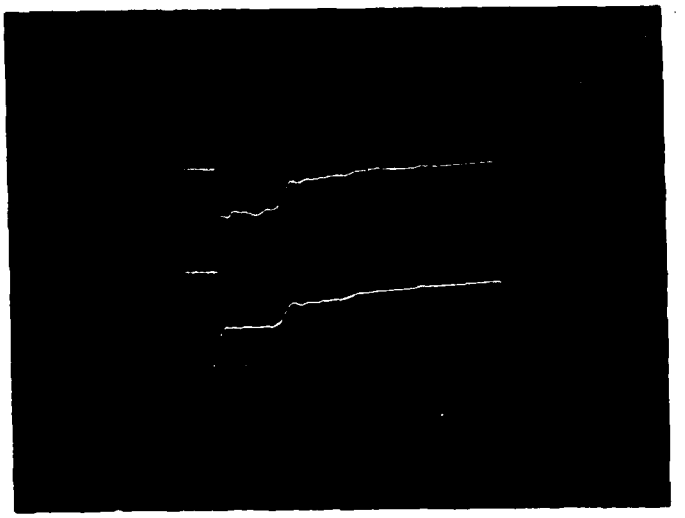

5 ms/div

III. Expanded 10 ms Burst (1 ms frames) for Composite Representation
Vert.: 20 mV/div.; Horiz.: 100 µs/div.

Flashlamp: 4.9kV

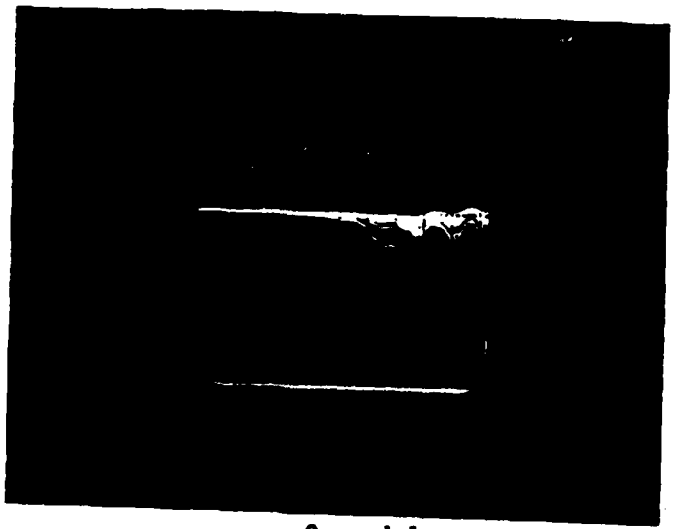

0 ms delay

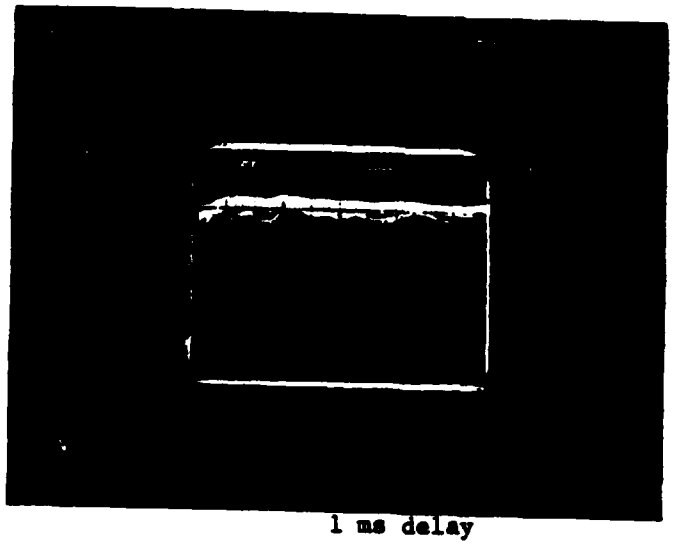

1 ms delay

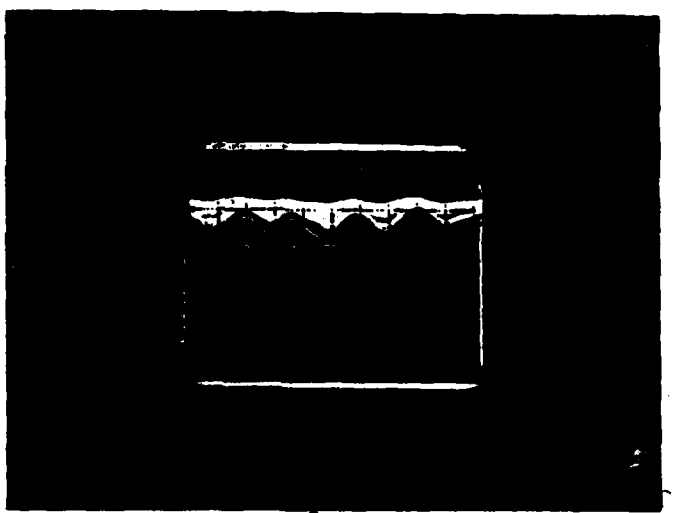

2 ms

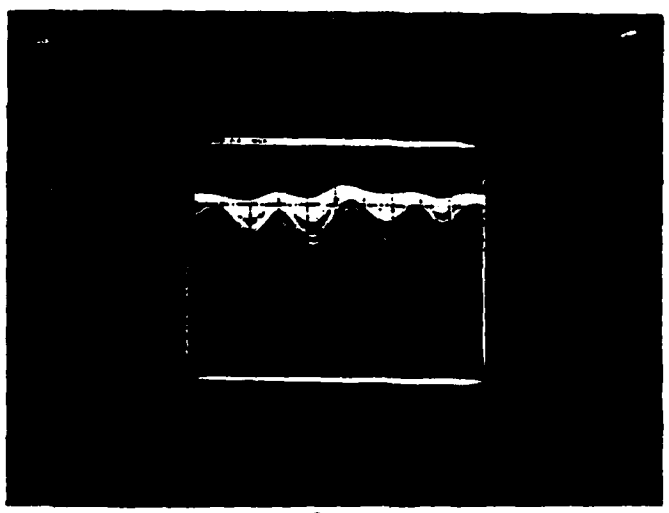

3 ms

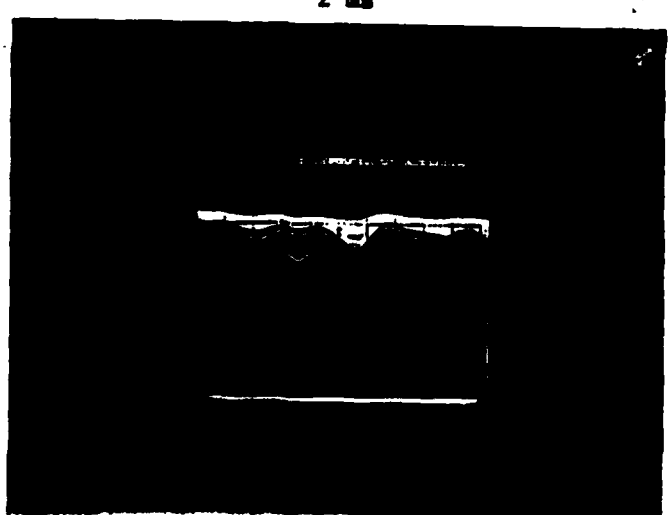

4 ms

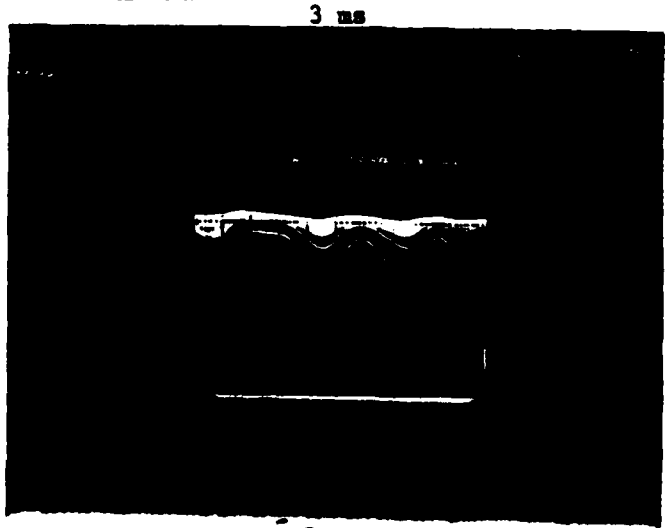

5 ms

IV. Effect of Voltage Increases

1 Capacitor/Flashlamp (1 ms discharge)

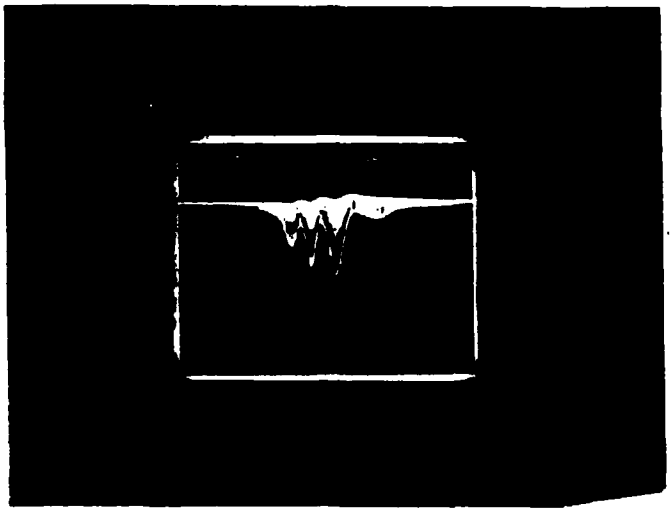

4.9 kV

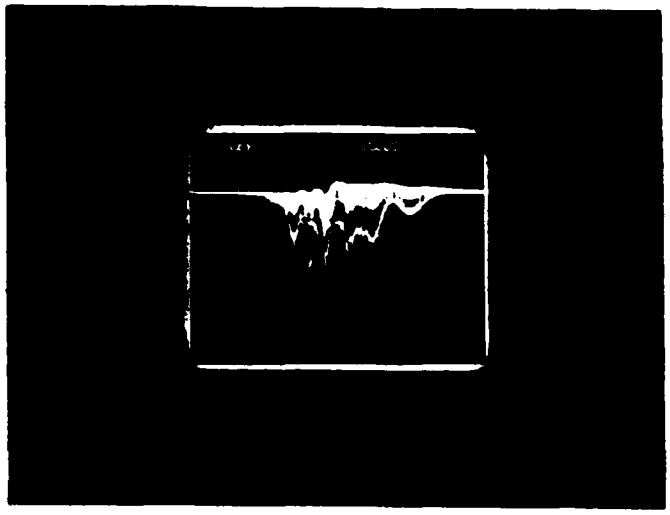

5.3 kV

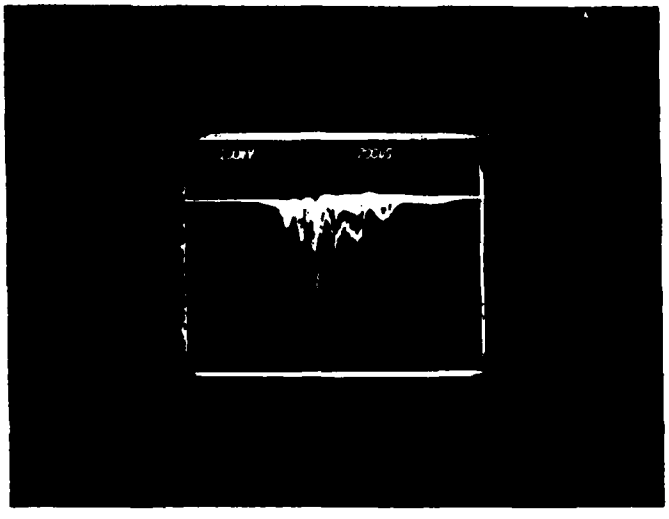

5.5 kV

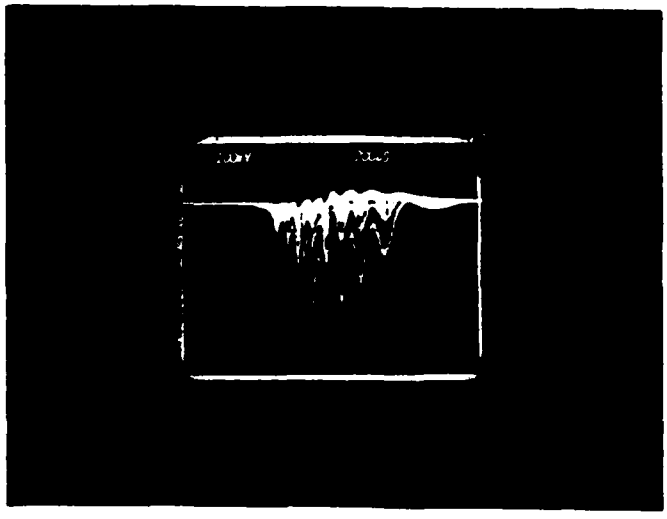

5.9 kV

APPENDIX F

DETECTION SYSTEMS

A study of various types of photodetectors and related electronics was made. The study concentrated on detectors and systems useful for diagnostics of the laser output and diagnostics of the gas after laser heating by observation of energy and temporal modifications to the beam. The major characteristic required of a detection system to do beam diagnostics is a rapid response, as the mode-locked pulses are only 100ps in width. Gas diagnostics require, in addition, that the detector have good sensitivity since scattering processes scatter only 10E-8 to 10E-3 of the incident radiation. The qualities of rapid response and good sensitivity tend to be mutually exclusive in detectors.

A general, nonexhaustive review of detectors, expanded from an article in the Laser Focus Buyer's Guide [1], is included as background for the discussion of some specific components.

There are three broad classes of detectors for the near-UV, visible, and near-IR spectral range, grouped according to detection process: Photoemissive, semiconductor, and thermal. Photoemissive detectors use the photoelectric effect, emitting electrons from a cathode when the cathode is struck by light. These electrons are the signal of light striking the detector. Photoemissive devices are vacuum photodiodes, photomultiplier tubes, and microchannel plates. Photomultiplier tubes have excellent sensitivity, however, the complexity of the tube slows the response time. To accurately reproduce a 100ps wide pulse requires a risetime (t_r) of about 30-40ps. Using the frequency bandwidth-rise-time relationship [2,3]

$$f = 0.35/t_r$$

a pulse with a 35 ps risetime would require a 10Ghz bandwidth detector. This also applies to other electronics in the system, as will be discussed later. For 1.06u light, the spectral response needed is (RCA) 73ER. The S-1 spectral response also has the required infared range, however, the 73ER response is about five times more sensitive at 1.06u. The fastest tube in the RCA inventory

with the 7JER response in the C31034D, with a risetime of 2.5ns. The C31034D has a quantum efficiency of 0.2% and an absolute responsibity of 2mA/W at 1.06u. A photomultiplier will respond to a light pulse much shorter than the FWHM of the tube, called a delta function pulse [4], however, the C31034D is not an entirely satisfactory solution because of the slow response, especially since the photomultiplier would be called on to respond to a train of pulses ions apart. There are photomultipliers on the market with a much shorter risetime, such as the Amperex XP 2020 (1.5ns), but these lack the required spectral response. [5] Microchannel plates have much better response times than photomultiplier tubes, having risetimes of 200-400ps, but the plate must look at a pulse train, and the time to read out the MCP (about a microsecond [6]) would limit it to single pulse use. A factor in deciding to look for a more suitable detector than a PM tube or a MCP is the extreme sensitivity, which would not be a problem in gas diagnostics, but which would require extreme care if laser beam diagnostics were done. Microchannel plates cost about $30,000 each, which is also an inhibiting factor in deciding whether to use them.

The second class of detector is the semiconductor detector. Semiconductor detectors operate because of the energy gap between the valence band and the conduction band. Energy from photons striking the detector raises electrons into the conduction band where they appear as a signal. There are two main types of semiconductor detectors, photodiodes and photoconductors. Photodiode detectors operate at a reverse bias. When light is incident on the detector, the detector becomes conductive with a constant resistance. This type of detector is sometimes call photovoltaic. Photoconductive detectors operate by varying detector resistance proportionally to varying light intensity. [7] Both types of dector can be vary fast because both types employ solid state processes. Solid state detectors are frequently made of silicon or germanium or a compound of one of these. Typical spectral response of these types is VIS-NIR (400-1100nm). Other detector materials include gallium arsenide, lead

sulfide, lead selenide, and others. See the attached table of spectral ranges of detector materials. [8] The photodetector chosen for initial operation beam diagnsotics is a Ford Aerospace silicon photomixer/laser detector diode L4501. This detector has a spectral range of 400-1100nm with peak response at 800nm and a risetime of 6-10ps. The detector is operated with a bias tee and a bias supply in the configuration shown below.

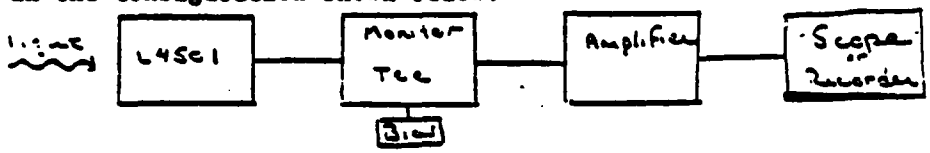

In a recent article in Laser Focus, S. Y. Wang described two GaAs Schottky photodiodes with very large bandwidths of 20GHz and 100GHz. [9] The 20GHz photodiode is a production model fabricated by Hewlett-Packard, and the 100GHz model is an experimental device in use of HP labs. The response time of these photodiodes is outstanding, however, the spectral response cuts off at 850nm. While these detectors are not suitable for 1.06u radiation, they are candidates for beam monitoring when the laser output is frequency doubled. It may not be necessary to employ a second detector type for doubled monitoring since the spectral range of the Ford photodiode extends to 400nm. S. Sarraf has suggested using an ITL TF1850 photodiode with an S-1 spectral response as a beam monitor. This would work to some extent, but the risetime of the TF1850 is 100ps and would distort the pulse shape considerably. [10] The TF1850 detector is also considerably more expensive than the L4501.

The third class of detector is the thermal detector. Calorimeters, pyroelectric detectors, and thermopiles are all versions of thermal detectors. Thermal detectors work by using temperature changes to create a signal. This is done in the case of thermopiles and calorimeters by using the thermoelectric effect, and in the case of pyroelectrics by measuring the signal produced when the polarization of a dielectric in a capacitor changes due to temperature change. The term "calorimeter" is sometimes used when talking about thermopile-type detectors, as both types are used as the basis for power and energy

measuring instruments. One technique which may be used is to calibrate a photodiode detector using a power/energy meter, then use the photodiode as a monitor of the beam energy. This technique would get around the inability of conventional meters to separate out a single 100ps pulse from a train of such pulses. Scientech Inc. has a line of thermopile-based power/energy meters, of which the 4" volume absorbing calorimeter combined with a power and energy indicator would work well. Other companies manufacturing similar devices are Gentech, Advanced Kinetics, and Apollo Lasers. This type of instrument is very common and should present no problems in terms of inability to meet specifications for energy measurement of this system. A pyroelectric detector was suggested as an energy monitoring device for the laser, but use of the photodiode should make this unnecessary. It should be noted that at Los Alamos National Laboratory a pyroelectric detector was made to function on a 10-35ps scale in conjunction with a LANL-built ocilloscope. [11] The reason (besides potential for fast response) the pyroelectric detector was chosen was because of its good room temperature response at 10.6u, a wavelength where semiconductor detectors often have excessive noise due to background infared radiation. The material chosen for the LANL system was strontium barium niobate (SBN). The article also talked about using another instrument to calibrate the detector to be used as the beam monitor. In the case of the LANL experiment, the device used to calibrate the detector was a streak camera.

The streak camera was purposely left out of the classification of detectors because it is more of a system than any of the detectors previously discussed. The streak camera operates much like a TV camera, and can obtain very good time resolution and very good sensitivity. Hamamatsu sells a streak camera system (Temporaldisperser) with resolution to 1ps. There is currently on loan to the laboratory a framing/streak camera made by Imacon with a resolution of about 150ps. The problem with purchasing a camera system is that streak cameras currently cost $40,000-$100,000. The operation of a camera as

a dector is tedious, making more attractive the idea of using the camera as a calibration tool for a separate detector.

With the detector a means is needed of recording the detector signal for analysis. The same limitations on bandwidth/risetime apply to the detector electronics as to the detectors themselves. A fudge to get around this require- will be explained later. The problem to be overcome (as with the detectors) is that the mode-locked pulses are extremely short and have a very short risetime. The frequency at which the pulses occur is 100MHZ (T=10ns) which is well within the response of many detectors and ocilloscopes. The frequency response required to respond without distortion to the individual pulses is about 10GHz, which is beyond the capability of any commercial ocilloscope or transit sampler today. There are two ways of recording the detector signal. The first method is to use a high speed ocilloscope and to photograph the trace. The fastest ocilloscope on the market today is the Tektronix 7104, with a bandwidth of 1GHz and a risetime of 350ps. This scope would display the mode-locked pulses, but would distort them considerably. There are sampling oscilloscopes which can accurately reproduce up to 14GHz signals, but these require a repetitive signal. The 1ms to 10ms pulse train is not long enough to allow the use of sampling, which samples parts of many pulses and produces a composite pulse with the same characteristics as the original signal. The fastest conventional oscilloscopes after the 7104 are 500MHz bandwidth scopes. This includes ocilloscopes produced by Hewlett-Packard and other companies. The second method for recording the signal is the use of a transient digitizer. These are manufactured by several companies, including Gould Biomation and Tektronix. The waveform digitizer is able to take an incoming signal and store it digitally for display or analysis. The fastest digitizer currently on the market is the Tektronic 7912AS Programable Transient Waveform Digitizer. This has a variable real time bandwidth from 650MHz to 1GHz, depending on the plug-ins used. The advantage of the digitizer is that the signal can be fed to a computer for correction

(of the bandwidth distortion) and for analysis of the signal itself. The 7912AD has a sampling rate which samples 512 times during a window 5ns to 10ms wide giving a sample spacing of 9.8ps to 19.5μs between samples. This is up to a 100GHz sampling rate. The analog response of the amplifier and other 7912AD electronics is not sufficient to amplify and accurately through out a signal with a frequency of 100GHz. The process which occurs is that the amplifier amplifies a signal and sends the signal to the sampling electronics. The sampling electronics makes a record of the voltage every 10ps (when operating at the maximum rate). If the frequency of the signal is beyond the bandwidth/ risetime of the rest of the system electronics, the sampling electronics will read the voltage each 10ps (max rate) of a signal which has been distorted, broadened, or poorly amplified to a greater of lesser extent which depends on the frequency of the original signal.

References

1. "Detectors," Laser Focus Buyer's Guide 1984 Penn Well Publishing Co, Mass., 1984, p. 281.

2. Wolpert, H. D., Photonics Spectra, 17, 12, 1983, p.71.

3. "Ocilloscope Reference," Tek Products 1984, Tektronix, Ore., 1984, p. 227.

4. Wolpert, H. D., Photonics Spectra, 17, 12, 1983, p. 71.

5. Leskovar, B., Laser Focus, 20, 2, 1984, p.73.

6. Leskovar, B., Laser Focus, 20, 2, 1984, p.73.

7. "Detectors," Laser Focus Buyer's Guide 1984, Penn Well Publishing Co., Mass, 1984, p. 281.

8. "Detectors," Laser Focus Buyer's Guide 1983, Penn Well Publishing Co., Mass, 1983, p. 448.

9. Wang, S. Y., Laser Focus, 19, 12, 1983, p. 99.

10. Sarraf, S., Private Communication.

11. McLellan, E. J., and Stotlar, S. C., Optical Spectra, 15, 3, 1981, p. 55.

Annual Report

on

ANALYTICAL MODELING OF STRONG RADIATION GAS-DYNAMIC INTERACTION

Submitted to:

Dr. L. H. Caveny
Air Force Office of Scientific Research
Directorate of Aerospace Sciences
Bolling Air Force Base, D.C. 20332

by

Dr. Charles L. Merkle
Mechanical Engineering Department
The Pennsylvania State University
University Park, PA 16802
814-863-1501

January 1985

b. Research Objectives

The aim of the analytical effort is to study the detailed mechanisms involved in laser-gasdynamic interactions to improve our understanding of the physical mechanisms involved. Specific aspects of this problem which were addressed include:

1. Verify the capability for obtaining two-dimensional numerical solutions. Continue to upgrade algorithm to improve reliability and convergence.

2. Calculate the rate of propagation of the absorption zone in an internal flow situation and estimate variations in absorption zone volume with dominant parameters in the laser propulsion problem including: laser power, intensity, f-number, gas constituents and absorptivity characteristics.

3. Develop a one-dimensional stability analysis of the laser-gasdynamic interaction and assess potential instabilities which may be encountered in experimental situations.

c. Status of Research Effort

Detailed modeling of laser-flowfield interactions is proceeding in three distinct, but related, directions. In the simplest, a one-dimensional analysis is being used. The second direction that is being pursued is the solution of the complete two-dimensional problem including the effects of arbitrary beam convergence and realistic cross-beam intensity profiles. The third area of analysis concerns the stability characteristics of the laser-gasdynamic interaction. Thus far, stability characteristics are being studied in only the one-dimensional approximation. These analyses all share a common numerical procedure.

The physical phenomena being modeled are indicated on Fig. 1. In particular, the analysis takes into account (equilibrium) real gas properties including specific heats, molecular weights, viscosity, conductivity and gas absorptivity. In the one-dimensional analysis the incoming radiation is constrained to be uniform across the passage and to converge at the same rate as the geometry. In the two-dimensional analysis the beam can be focused at an arbitrary point, and can have an arbitrary cross-stream intensity profile. The stability analysis considers the amplification of infinitesimal disturbances by the laser-gasdynamic interaction with the intent of illucidating the dynamic behaviors of these interactions.

During the present twelve months, a parametric study of the one-dimensional interaction was begun. Previous work had included representative one-dimensional solutions, but no systematic studies. Representative results were reported in Ref. d7 which showed that the mass flow through a one-dimensional nozzle with laser heat addition could attain multiple values. This arises because of a hysteresis loop that is

encountered as laser power is first increased to high levels and then reduced to low values. At low powers, laser absorption is very low, but above a particular power level the fractional power absorbed jumps to high levels (approaching 100%). As power is lowered again, this high fractional absorption persists until substantially lower powers at which point it again abruptly goes "out", thus creating a region of multiple solutions. Similar studies of the effect of inlet temperature show similar substantial changes in fractional power absorption with changes in the inlet temperature. Some representative results of this nature are shown on Fig. 2.

The first-ever two-dimensional calculations which couple the effects of a variable gas absorptivity to a flowing gas were also completed during the present year. (Some previous two-dimensional results for a constant absorptivity gas were reported in Ref. d6.) In these calculations, the absorptivity of hydrogen with 1% Cs seedant was used. Representative temperature contours for a series of laser powers are shown in Fig. 3. One of the characteristics noted in the two-dimensional flow is that the central portion of a gaussian beam is absorbed more rapidly than the outer portion so that the peak intensity at downstream stations occurs off-axis, as shown in Fig. 4. The two-dimensional results show that the strongest gradients are in the radial (not the axial) direction and that gas flow rates are completely independent of the one-dimensional eigenvalue solutions.

Results of the one-dimensional stability characteristics of a laser-gasdynamic interaction were also calculated during the subject reporting period. These results show that disturbances are amplified in a converging nozzle for almost all conditions, but that this amplification is

weak and is offset by the available damping at other points in the nozzle. Some representative growth/decay curves for disturbances of one wavelength are given in Fig. 5. Other results were reported in Ref. d7.

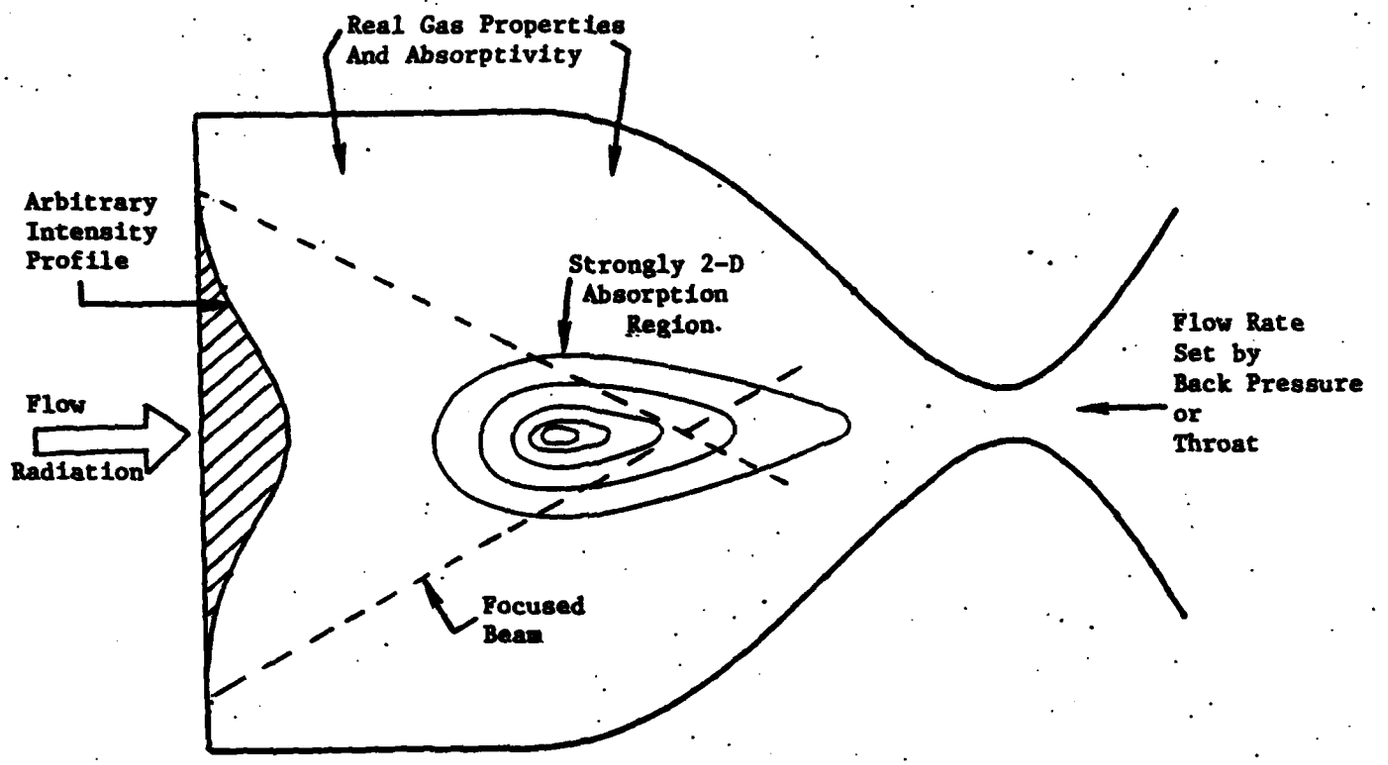

Fig. 1. Physical Phenomena Included in Model of Laser-Gasdynamic Interaction

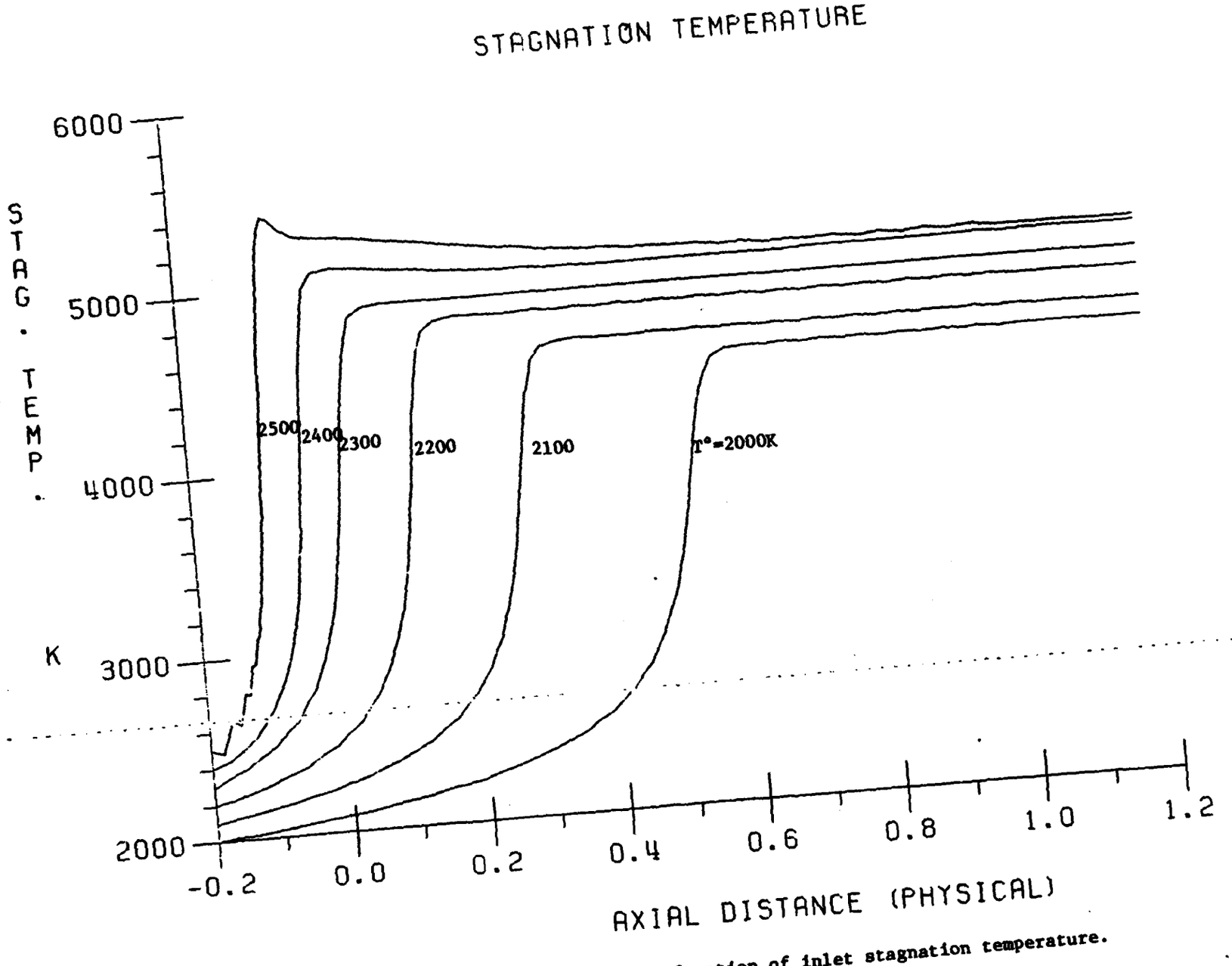

Fig. 2. Temperature distribution as a function of inlet stagnation temperature. Inlet power 10^8 W/m.

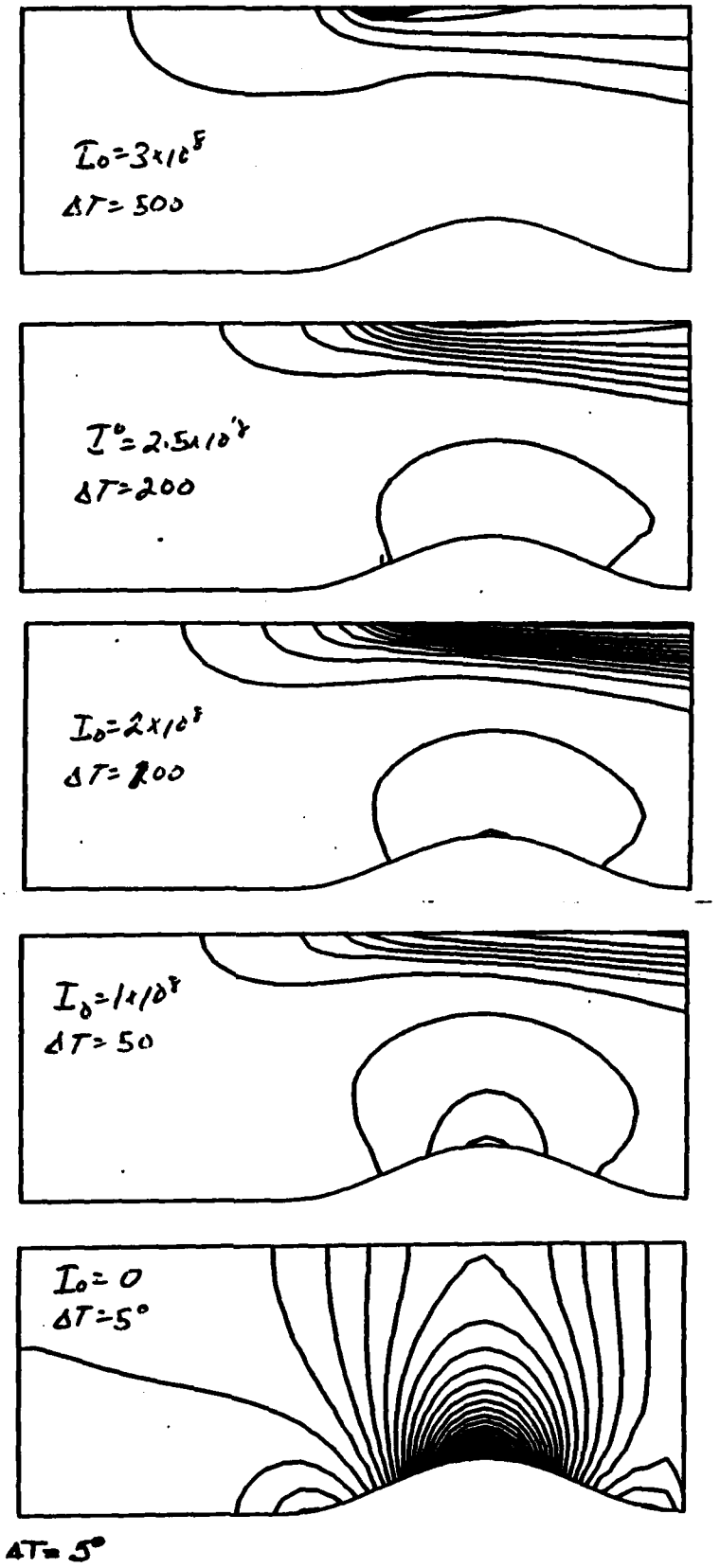

Figure 3. Temperature Contours for Laser Heat Addition. Flow from Left to Right.

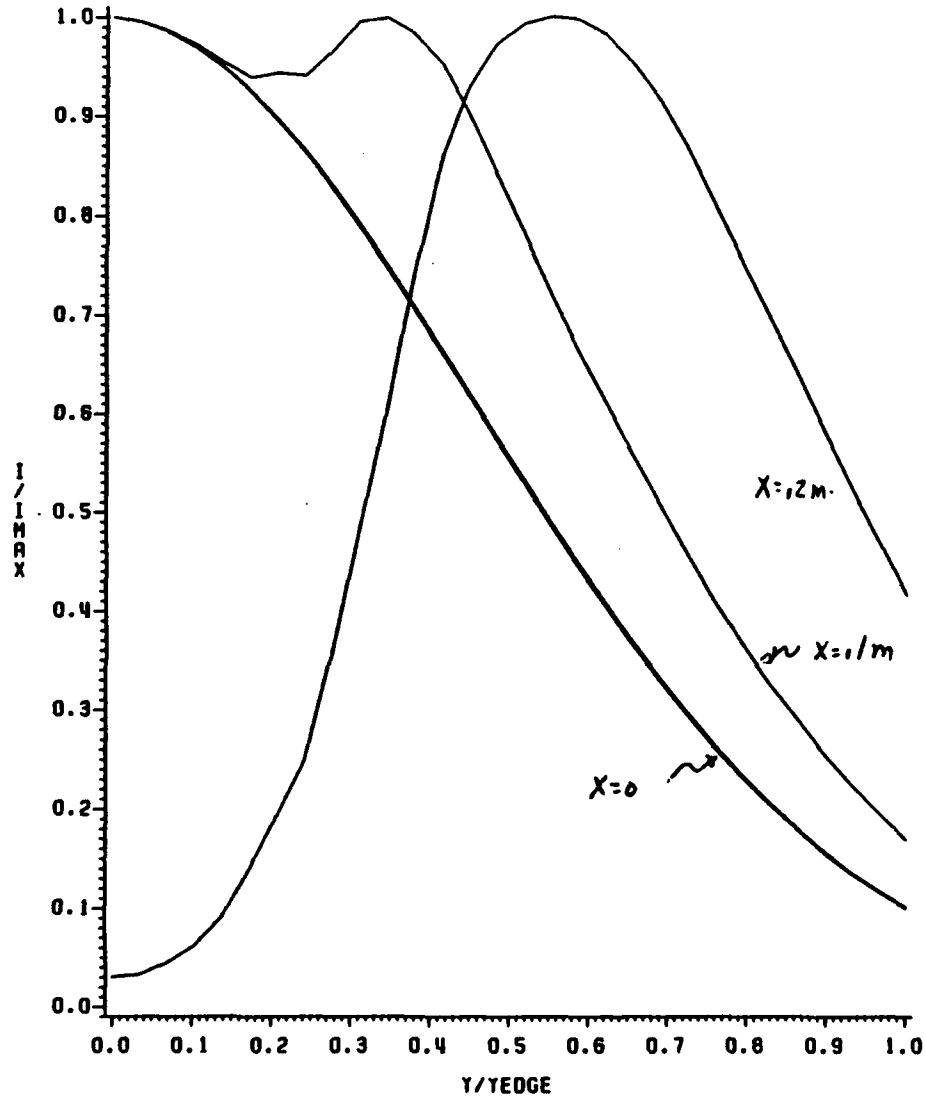

Figure 4. Laser Intensity Profiles at Several Axial Locations

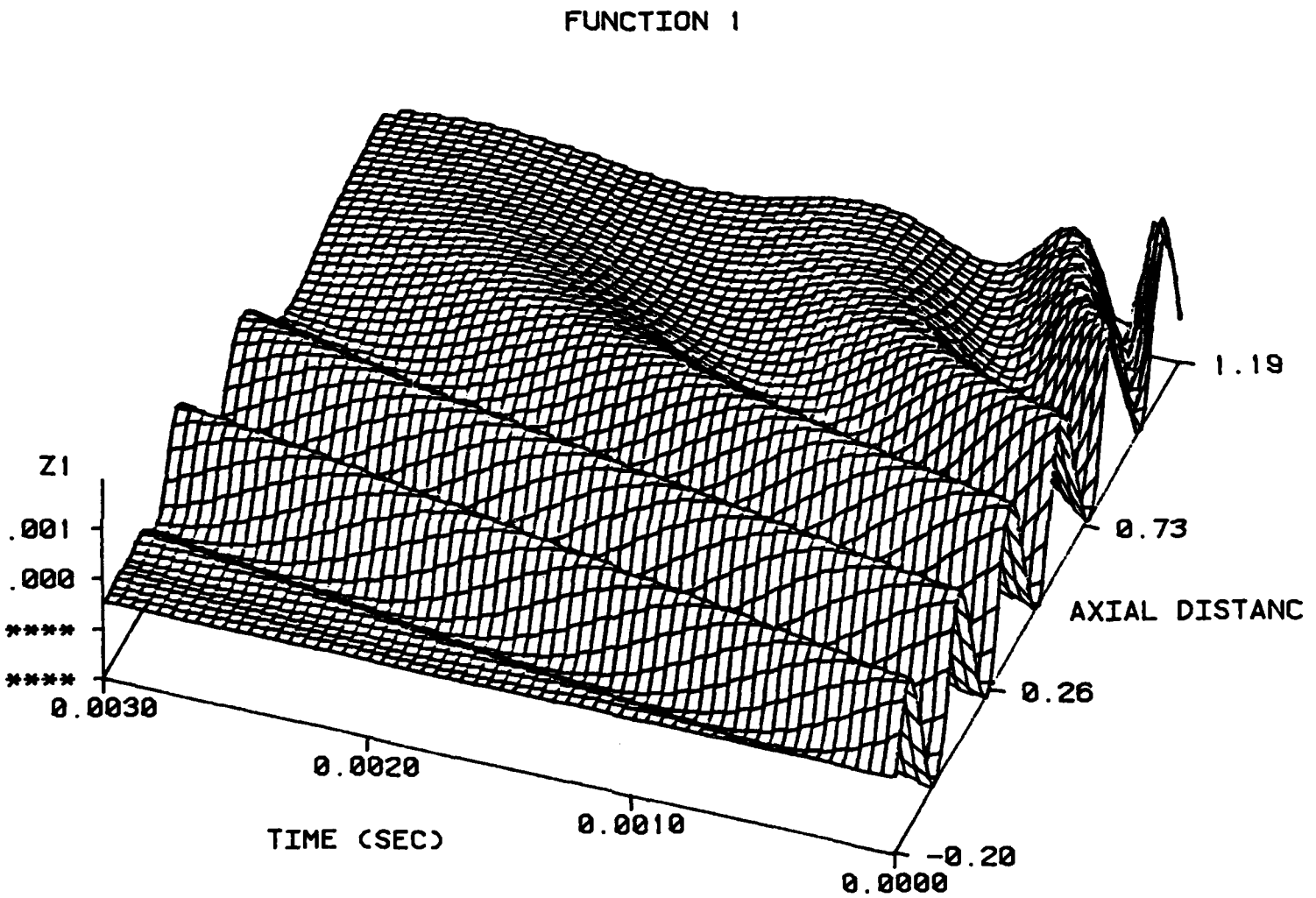

Fig. 5. Growth and damping of a semisoidal disturbance in a one-dimensional laser absorption engine.

d. A Cumulative Chronological List of Written Publications in Technical Journals

1. Merkle, C. L. and Gulati, A., "The Absorption of Electromagnetic Radiation in an Advanced Propulsion System," J. Spacecrafts and Rockets, Vol. 21, No. 1, Jan.-Feb. 1984, pp. 101-107.

2. Merkle, C. L., "The Potential for Using Laser Radiation to Supply Energy for Propulsion," Orbit Raising and Maneuvering Propulsion: Research Status and Needs, AIAA Progress in Astronautics and Aeronautics Series, L. H. Caveny, Ed., AIAA, New York, 1984, pp. 48-72.

3. Merkle, C. L., "The Use of Electromagnetic Radiation as an Energy Source for Propulsion," Proceedings of Workshop on Advanced Propulsion Concepts Using Time Varying Electromagnetic Fields, Michigan State University Press, 1984.

4. Merkle, C. L., "Prediction of the Flowfield in Laser Propulsion Devices," AIAA Paper 83-1445, AIAA 18th Thermophysics Conference, Montreal Canada, May 1983. AIAA Journal, Vol. 22, No. 8, Aug. 1984, pp. 1101-1107.

5. Merkle, C. L. and Gulati, A., "The Effect of Strong Heat Addition on the Convergence of Implicit Schemes," AIAA Paper 83-1914, AIAA 6th Computational Fluid Dynamics Conference Proceedings, Danvers, MA, July 1983. To appear, AIAA Journal, June 1985.

6. Merkle, C. L., Molvik, G. A. and Choi, D., "A Two-Dimensional Analysis of Laser Heat Addition in Converging Nozzles," AIAA Paper 84-0529, AIAA Aerospace Sciences Meeting, Reno, NV, Jan. 1984. To appear, AIAA Journal July 1985.

7. Merkle, C. L., "Stability of Absorption of Phenomena in Laser-Thermal Propulsion Gasdynamic Interaction," AIAA Paper 84-1571, AIAA 17th Fluid Dynamics, Plasmadynamics & Lasers Conference, Snowmass, CO, June 1984.

e. Professional Personnel Associated with Research Effort

Professional Staff -

Charles L. Merkle, Principal Investigator, Professor, Mechanical Engineering

Graduate Students -

Michael J. Stanek, Graduate Assistant, February 1981-August 1982. M.S. Thesis title, "Analytical Studies of the Absorption Mechanisms of Equilibrium Hydrogen." Present position: Lieutenant, US Air Force, AFWAL/POTC, WPAFB, OH.

Anil Gulati, Graduate Assistant, September 1981-August 1983. M.S. Thesis title, "The Absorption of Electromagnetic Radiation in an Advanced Propulsion System." Present position: Ph.D. Candidate, Dept. of Aerospace Engineering, U. Michigan, Ann Arbor, MI.

Gregory A. Molvik, Graduate Assistant, M.S. 1984, Present address: CFD Group, NASA/Ames, Moffett Field, CA.

Peter Tsai, Graduate Assistant, September 1983-Present. Anticipated M.S. Thesis, "Stability Characteristics of Laser-Supported Plasmas."

f.1. Interactions (Spoken Papers)

"Analysis of Laser-Supported Combustion Waves in Flowing Media," AFOSR/AFRPL Rocket Propulsion Research Meeting, Lancaster, CA, March 26, 1981.

"The Potential for Using Laser Radiation as an Energy Source for Propulsion," Orbit Raising Propulsion Workshop, Orlando, FL, January 16, 1982.

"The Use of Electromagnetic Radiation as an Energy Source for Propulsion," Symposium on Advanced Propulsion Concepts Using Time-Varying Electromagnetic Fields, East Lansing, MI, February 4, 1982.

"Analysis of Laser-Supported Plasmas in Flowing Media," AFOSR/AFRPL Rocket Propulsion Research Meeting, Lancaster, CA, March 3, 1982.

"The Absorption of Electromagnetic Radiation in an Advanced Propulsion System," AIAA Electric Propulsion Meeting, New Orleans, LA, November 19, 1982.

"Prediction of the Flowfield in Laser Propulsion Devices," AIAA 18th Thermophysics Conference, Montreal, Canada, May 1983.

"The Effect of Strong Heat Addition on the Convergence of Implicit Schemes," AIAA 6th CFD Conference, Danvers, MA, June 1983.

"A Two-Dimensional Analysis of Laser Heat Addition in Converging Nozzles," AIAA Aerospace Sciences Meeting, Reno, NV, January 1984.

"Stability of Absorption Phenomena in Laser-Thermal Propulsion Gasdynamic Interaction," AIAA 17th Fluid Dynamics, Plasmadynamics & Lasers Conference, Snowmass, CO, June 25-27, 1984.

"High Power Nd-Glass Laser Instrument for Advanced Propulsion and Diagnostics", AFOSR/AFRPL Rocket Propulsion Research Meeting, Lancaster, CA, March 12-15, 1984.

f.2. Interactions (Advisory Functions)

Member of Workshop Panel, "Concepts and Experiments," NASA/Michigan State Symposium on Advanced Propulsion Concepts Using Time-Varying Electromagnetic Fields, February 1982.

"Aerospace Propulsion at Penn State," presentation to General Robert T. Marsh, USAF, The Pennsylvania State University, University Park, PA, May 5, 1982.

g/h. New Discoveries and Other Statements

The first two-dimensional solutions of the interaction between a laser beam and a flowing gas have been obtained. These results afford substantial new understanding of the laser absorption process. The results show that radial gradients arising near the edge of the converging beam are stronger than axial gradients, thus indicating that the earlier approximate one-dimensional analyses for this problem are complete incorrect. The mass flow through the absorption zone can also take on nearly any value and is not restricted to a unique eigenvalue as suggested by these earlier models. The results also show that the fraction of power absorbed is maximized by proper selection of the incoming power, the mass flow and the pressure level in the nozzle. The power remaining in an initial gaussian beam is likely to be concentrated near the outer edges of the beam as the central part of the beam is absorbed most readily. The two-dimensional results also suggest substantial amounts of energy can be absorbed in the diverging portion of the beam.

The stability results are all one-dimensional in nature and must be considered as qualitative at best, but they represent the most complete study of the stability problem. The results show that heat addition in a converging nozzle provides a proper environment for amplification of disturbances, but in the one-dimensional analysis, this amplification does not appear to cause difficulties except in limiting cases of very high powers where instabilities may prevent a stable solution.

END

FILMED

7-85

DTIC